Repression of apelin Furin cleavage sites provides antimetastatic strategy in colorectal cancer

Béatrice Demoures, Fabienne Soulet, Jean Descarpentrie, Isabel Galeano-Otero, José Sanchez Collado, Maria Casado, Tarik Smani, Alvaro González, Isabel Alves, Fabrice Lalloué, et al.

Repression of Furin cleavage sites of apelin provides antimetastatic strategy in colorectal cancer.

Béatrice Demours[1], Fabienne Soulet[1], Jean Descarpentrie[1], Isabel Galeano-Otero[1], José Sanchez Collado[1], Maria Casado[1,2], Tarik Smani,[3] Alvaro González[1], Isabel Alves[4], Fabrice Lalloué[5], Bernard Masri[6], Estelle Rascol[4], Jean-William Dupuy[7], Cyril Dourthe[7], Frédéric Saltel[1,7], Anne-Aurélie Raymond[1,7], Iker Badiola[2], Serge Evrard[1,8], Bruno Villoutreix[9], Simon Pernot[1,8], Géraldine Siegfried[1*], Abdel-Majid Khatib[1*]

[1] University of Bordeaux, Bordeaux Institute of Oncology (BRIC)-UMR1312 Bordeaux, France

[2] Department of Cell Biology and Histology, University of the Basque Country, Bº Sarriena sn 48940 Leioa Spain

[3] Institute of Biomedicine of Seville, University Hospital of Virgen del Rocío/University of Seville/CSIC, Avenida Manuel Siurot s/n, 41013 Seville, Spain.

[4]Univ. Bordeaux, CNRS, Bordeaux INP, CBMN, France

[5]EA3842- CAPTuR, GEIST, Faculté de Médecine , Université de Limoges , 2 rue du Dr Marcland , 87025 Limoges Cedex , France.

[6] Institut Cochin, INSERM U1016, CNRS UMR 8104, Université Paris Cité, 75014 Paris, France.

[7] Oncoprot Platform, TBM-Core US 005, Bordeaux, France.

[8] Institut Bergonié, Bordeaux, France

[9] Université de Paris, Inserm UMR 1141, Robert-Debré Hospital, 75019 Paris, France.

Running title: Apelin cleavage sites in cancer

Total characters count: 14785words

[*] **Corresponding authors**
Abdel-Majid Khatib,
E-mail: majid.khatib@inserm.fr
Géraldine Siegfried
E-mail: Geraldine.siegfried@inserm.fr
Tel : 33-675243164
Bordeaux Institute of Oncology (BRIC),
UMR1312 Inserm, B2 Ouest,
Allée Geoffroy St Hilaire CS50023, 33615,
Pessac, France

Abstract

The adipokine apelin has been directly implicated in various physiological processes during embryogenesis and human cancers. Nevertheless, the importance of the conversion of its precursor proapelin to mature apelin in tumorigenesis remains unknown. In this study, we identify Furin as the cellular proprotein convertase responsible for proapelin cleavage. We explore the therapeutic potential of targeting proapelin cleavage sites in metastatic colorectal cancer by introducing apelin-dm, a modified variant resulting from alteration in proapelin cleavage sites. Apelin-dm demonstrates efficacy in inhibiting tumor growth, promoting cell death, suppressing angiogenesis, and early colorectal liver metastasis events. Proteomic analysis reveals reciprocal regulation between apelin and apelin-dm on proteins associated with clinical outcomes in colon cancer patients. Apelin-dm emerges as a modulator of apelin receptor dynamics, influencing affinity, internalization, and repression of apelin signaling linked to various protein kinases. Pharmacokinetic and toxicity assessments confirm the specificity, safety, and stability of apelin-dm, as well as its facile hepatic metabolism. These findings position targeting proapelin cleavage as a promising therapeutic strategy against metastatic colorectal cancer, paving the way for further clinical exploration.

Key words: Apelin / Furin / colon cancer/ liver metastasis/ safety pharmacology.

Introduction

Colorectal cancer (CRC) stands as the second leading cause of cancer-related mortality worldwide and ranks third in global cancer diagnoses (Morgan *et al*, 2023). Despite the efficacy of surgical resection and adjuvant treatments in early-stage disease, relapse and metastasis remain common. The prognosis of CRC is significantly influenced by local tumor staging, with liver metastasis being the predominant occurrence, followed by the lung. Approximately one in five CRC patients presents with liver metastases at diagnosis, and up to half will develop liver metastasis during the disease course (Siriwardena *et al*, 2014). Early detection of colorectal liver metastasis (mCRC) is paramount for improving survival rates, enabling the selection of candidates for curative liver surgery, and guiding treatment decisions.

Apelin, a bioactive peptide initially discovered in the gastrointestinal tract, plays a key role in regulating various physiological functions through its interaction with the G-protein-coupled apelin receptor (Read *et al*, 2019). Apelin stands at the crossroads of physiological responses, exhibiting heightened expression under hypoxic conditions. Beyond its established roles in promoting epithelial cell growth, proliferation, and migration (Bernier-Latmani *et al*, 2022; Wang *et al*, 2004), apelin has emerged as a key player in the pathophysiology of metabolic and cardiovascular diseases (Palmer *et al*, 2022). This peptide's involvement in cancer is expansive, with documented expressions in various cancers. Apelin overexpression notably correlates with increased tumor growth and microvessel density across diverse cancer types (Bernier-Latmani *et al*, 2022; Zuurbier *et al*, 2017; Lv *et al*, 2022; Picault *et al*, 2014a; Gourgue *et al*, 2020). In colorectal cancer, apelin concentration becomes a predictive indicator, influencing responses to bevacizumab therapy and affecting susceptibility to apoptosis-inducing agents (Zuurbier *et al*, 2017).

The cDNA of apelin encodes a 77-amino-acid (aa). The apelin peptides isolated from different tissues and cell types suggest that they are processing products derived from the C-terminal portion of this peptide precursor. The main active forms of apelin are apelin-13 aa, apelin-17 aa, and apelin-36 aa (or proapelin). Apelin-36 is directly generated from pre-proapelin (55 aa) by unknown proteases (s) (Lee *et al*, 2000; B *et al*, 2002). Subsequently, apelin-36 is rapidely cleaved within the two dibasic conserved sequence motifs RRK60F and RR64QR to generate apelin-17 and apelin-13, respectively (**Fig. 1A, Appendix Figure S1A**), suggesting the involvement of proprotein convertases (PCs) in this process (Seidah & Prat, 2012; Siegfried *et al*, 2020; Scamuffa *et al*, 2008). This study reveals Furin as a unique cellular apelin precursor cleaving enzyme, uncovering potential clinical significance of unprocessed proapelin, designated apelin-dm, obtained by Furin cleavage sites mutations. When expressed in colon cancer cells or administered pharmacologically to mice with colon cancer tumors, apelin-dm represses the malignant and metastatic phenotype of cancer cells. Apelin-dm altered apelin receptor internalization and signaling and directly competed with apelin and Elabela for apelin receptor binding and activation. Investigation of apelin-dm peptide in a panel of Absorption, Distribution, Metabolism, Excretion (ADME), toxicity assays, and pharmacokinetic profiles demonstrated its good safety profile, specificity, and stability in mice and human serum. This highlights apelin-dm as a promising and safe therapeutic strategy for colorectal cancer and its associated metastatic liver events, paving the way for targeted clinical interventions.

Results

Apelin precursor is specifically cleaved by the proprotein convertase Furin

To identify proprotein convertases (PCs) cleaving proapelin, coding region of proapelin was cloned from HUVEC and tagged with a V5 sequence for detection **(Fig. 1A)**. Co-transfection of LoVo cells, a PC-deficient cell line (Takahashi *et al*, 1993) with proapelin and various PC-encoding vectors revealed Furin's exclusive role in reducing apelin-55 and apelin-36 levels while generating apelin-17 and apelin-13 **(Fig. 1B)**. Co-transfection of CHO-FD11, cells with reduced Furin activity (Gordon *et al*, 1997) with proapelin and Furin resulted in decreased apelin-17 and increased apelin-13 secretion **(Fig. 1C)**.

To assess the efficiency of PC inhibitors on proapelin processing by endogenous Furin, we treated HEK293A cells with the synthetic Furin inhibitor decanoyl-Arg-Val-Lys-Arg-chloromethyl-ketone (CMK, 10 μM) (Seidah & Prat, 2012; Bontemps *et al*, 2007) or expressed in these cells the Furin inhibitors, including the Furin prodoamine (P-p-Furin) (Scamuffa *et al*, 2014) and α1-PDX (Descarpentrie *et al*, 2022; Jean *et al*, 1998) **(Fig. 1D)**. As demonstrated by Western blot analysis, transfection of HEK293A cells with a vector encoding proapelin (Control) resulted in ~95% processing. Treatment of cells with CMK or cotransfection with Furin inhibitors revealed that processing of proapelin is significantly blocked by CMK (~10% processing) and α1-PDX (~50% procession), P-p-Furin (~30% processing). In contrast, wild-type α1-antitrypsin failed to inhibit proapelin processing **(Fig. 1D)**. *In vitro* enzymatic assays (Sfaxi *et al*, 2014; Basak *et al*, 2010) confirmed increased enzymatic activity with PCs expression and its reduction by Furin inhibitors expression **(Appendix Figure S1B)**, supporting Furin as primary PC mediating proapelin cleavage, producing apelin-17 and apelin-13.

Apelin, apelin receptor, and Furin expression is altered in colorectal cancer and colorectral liver metastases

In a healthy colon, crypts contain stem cells responsible for the constant renewal and differentiation of the epithelial lining. While in cancerous tissue, these processes are disrupted, leading to uncontrolled cell proliferation, aberrant differentiation, and loss of normal crypt architecture (Humphries & Wright, 2008). Given the co-expression of apelin, apelin receptor and Furin, that we identified in colon tissues, colon carcinoma cells, and endothelial cells **(Appendix Figure S2)**, we sought to evaluate their expression and colocalization in both normal and colon cancer tissues. To do this, we first conducted immunohistochemical staining on a set of matched tissue sections, including normal human colon mucosa, primary colon tumors, and corresponding colorectal liver metastases from 35 patients. All these proteins were expressed in non-cancerous colon tissues, primarily localized to the base of the colon crypts **(Fig. 1E, F)**. The expression of apelin, apelin receptor and Furin in the colon crypts highlights their potential roles in maintaining the dynamic environment of the intestinal epithelium. In cancerous tissues, the loss of crypts was associated with a modified expression pattern of apelin, apelin receptor, and Furin, suggesting that these molecules may play roles in tumor progression and possibly in the tumor microenvironment. Quantitative analysis of immunohistochemistry staining in primary colorectal cancer (CRC) and metastatic colorectal cancer (mCRC) tumors, along with their respective normal colon tissues, revealed a consistent increase in the average staining levels of these proteins in the analyzed tumors **(Appendix Figure S3)**. Moderate correlation coefficients (ranging from 0.3 to 0.5) were observed between the expression levels of apelin and KI-67, apelin receptor and KI-67, as well as Furin and KI-67 in primary CRC **(Fig. 1I)** and their corresponding metastatic liver lesions **(Fig. 1J)**. These positive correlations underscore the potential roles of apelin, apelin receptor, and Furin in CRC progression and metastasis. Although apelin mRNA was overexpressed in CRC tumors and their corresponding metastatic livers, the average tumoral/normal (T/N) ratio of apelin expression in hepatic metastases was almost similar to that of colon primary tumors **(Fig. 1K)**. Furthermore, apelin receptor **(Fig. 1L)** and Furin **(Fig.**

1M) were overexpressed in metastatic tumors, with levels higher than those in matched healthy and primary colon tumors.

Hypoxia is a common feature of the microenvironment in almost all solid tumors and is frequently associated with angiogenesis and cancer growth, including CRC (Chen *et al*, 2023) and has been reported to induce apelin expression in endothelial cells (Andersen *et al*, 2011). Analysis of Furin expression in endothelial cells cultured under normoxic (21% O2) and hypoxic (1% O2) conditions revealed that hypoxia is also a strong inducer of Furin mRNA in endothelial cells, with increased expression observed at all tested hypoxia exposure times ranging from 4 to 24 hours **(Fig. 1N)**. Taken together, these findings indicate that the increased co-expression levels of apelin, the apelin receptor, and/or Furin are associated with CRC tumors, suggesting a potential role for these proteins in colon cancer progression and metastasis.

Alteration of proapelin cleavage sites contributes to the reduction of colorectal tumor growth and liver metastasis.

To investigate the functional significance of apelin precursor processing by Furin in colon cancer, we mutated the proapelin cleavage sites from RR60KFRR64QR to SS60KFSS64QR, creating the apelin double mutant (apelin-dm) **(Fig. 2A)**. Lentiviral vectors carrying mock, APLN , and APLN-DM were then introduced into colon cancer cell lines CT-26 and MC-38 **(Appendix Figure S4A)**. Despite Furin presence, the mutations prevent apelin-dm processing **(Fig. 2A)**. Wild-type APLN expression in cancer cells led to twofold increased anchorage-independent growth, while APLN-DM reduced proliferation and showed >80% decrease **(Appendix Figure S4B, C)**. APLN expression prevented induced apoptosis, unlike APLN-DM **(Appendix Figure S4D)**. In vivo tumor growth assay in Rag2/γc mice showed apelin increased growth, while apelin-dm significantly reduced it **(Fig. 2B, C)**. Apelin-dm also inhibited tumor growth in syngeneic BALB/c and C57BL/6 mice **(Fig. 2D, E)**, using both CT-26 and MC-38 cells. The expression of APLN-DM in these cells seems to affect their ability to mediate tumor

growth with varying efficacy. Indeed, a greater inhibitory effect was observed in CT-26 cells compared to MC-38 cells, suggesting the potential implication of genetic background differences in the mice used and/or differences in the tumorigenic mediators secreted by CT-26 and MC-38 in their tumor microenvironments. Additionally, MC-38 cells produce more apelin compared to CT-26 cells **(Appendix Figure S4A)**, suggesting the potential involvement of one or more of these differences in the lower anti-tumor efficacy of APLN-DM expression in MC-38 cells compared to CT-26 cells. Similarly, overexpression of APLN in MC-38 and CT-26 cells increased their ability to induce hepatic metastases and incidence, which is suppressed by APLN-DM expression **(Fig. 2F,G)**. Notably, APLN-DM-expressing cell-derived tumors exhibited a significant decrease in KI-67+ cells **(Fig. 2H, I, J)**. Taken together, these findings suggest that apelin-dm represses tumor growth, angiogenesis, and liver metastasis that are otherwise promoted by apelin.

Apelin-dm inversely regulates a protein subset induced by apelin, impacting clinical outcomes in colon cancer.

To identify the pathways mediated by apelin-dm involved in the repression of the malignant phenotype of colon cancer cells, we performed proteome analysis of cancer cells and the same cells expressing APLN and APLN-DM. Out of the 1825 cellular proteins identified, the expression of APLN and APLN-DM in cancer cells significantly increased the expression of only 14 and 153 proteins, and decreased 20 and 67 proteins, respectively **(Fig. 2K)**. Further analysis revealed that the most significantly dysregulated proteins in response to APLN and APLN-DM expression in cancer cells were related to extracellular matrix regulation, metabolic activity, cytokine production, cell death, and growth (**Appendix Table S1**). In cells expressing APLN-DM, the most induced proteins are single-stranded interacting protein 2 (Rbms2) and RNA-binding motif (RBP). Rbms2 is a tumor suppressor gene that inhibits cell proliferation by positively regulating the stability of P21, mediates cell apoptosis, and enhancing sensitivity to

several cancer treatments (Xu *et al*, 2022; Sun *et al*, 2018). The protein most repressed in apelin-dm-expressing cells was the oncogene GTPase NRas. Importantly, we found that 28 proteins were inversely regulated in cells expressing APLN and APLN-DM **(Fig. 2L)**. Several of these proteins were linked to both good and poor prognosis in colon cancer patients. Indeed, Galectin-3-binding protein (LGALS3BP), gelsolin (Gsn), and Spartin (Spg20), which are associated with a favorable clinical outcome in colorectal carcinoma are downregulated in APLN-expressing cells and upregulated in APLN-DM-expressing cells. In contrast, ATP-dependent RNA helicase (DHX36), Synembryn-A (Ric8a), Protein CYR61 (Cyr61), Tubulin alpha-1A (Tuba1a), and probable 28S rRNA (cytosine-C(5))-methyltransferase (NSUN5), which are associated with poor prognosis in colon cancer, are upregulated in APLN-expressing cells and downregulated in APLN-DM-expressing cells. Further analysis revealed that LGALS3BP expression was most affected by APLN-DM (~9.5-fold increase, **Appendix Table S1**). LGALS3BP has anti-tumor activity in colon cancer by suppressing Wnt signaling (Piccolo *et al*, 2015) and also plays a role in preventing and treating inflammatory diseases by suppressing TAK1-dependent NF-κB activation (Hong *et al*, 2019). Therefore, based on the ability of APLN-DM to regulate the expression of proteins involved in both good and poor prognosis of colon cancer patients, we used the web server GEPIA (http://gepia.cancer-pku.cn/) (Tang *et al*, 2017) to analyze their expression in colon cancer patients. We found that Gsn and Spg20 mRNA expression was significantly lower, and NSUN5 mRNA expression was significantly higher in colon tumor tissues than in normal tissues **(Fig. 2M)**. The same analysis also revealed upregulated expression of APLN and APLNR in colon cancer tumors **(Fig. 2M)**. We next explored the correlation between the expression of APLN and APLNR with genes that are dysregulated by APLN or APLN-DM expression in cancer cells, and involved in prognosis of colon cancer patients. Among the dysregulated molecules, we observed varying degrees of correlation with APLN and APLN-R. Specifically, we found a low positive correlation between APLN and CYR61 (r = 0.16), a stronger correlation between APLNR and CYR61 (r = 0.68), a

low correlation between APLNR and RIC8A (r = 0.20), and a moderate correlation between APLNR and TUBA1A (r = 0.58) in tumor patients **(Fig. 2N)**. Collectively, these results indicate that APLN-DM induces the expression of proteins associated with a favorable clinical outcome and limits the expression of proteins induced by APLN that are involved in the poor prognosis of colon cancer **(Fig. 2O)**.

Apelin-dm peptide represses apelin-mediated vascular network and tumor cells malignant phenotype

We next synthesized the apelin-dm peptide to explore its therapeutic potential. In apelin-36, the sequence "*RR*KF*RR*" has been substituted with "*SS*KF*SS*", where the R residues have been replaced by S. R is positively charged at neutral pH with approximate molecular (MW) of 174.2 Da. Whereas S is neutral with MW of 105.1 Da. This difference in molecular weight and charge properties likely contributes to the lower migration of apelin-dm peptide on SDS-PAGE than apelin-36 **(Fig. 3A, B)**. First, the impact of varying concentrations of apelin-dm on in vitro angiogenesis was assessed through a tube-like structure formation assay **(Appendix Figure S5A, B)**. This assay, which evaluated both the number of junctions and tubule length, revealed that apelin-dm disrupted the formation of capillary-like structures in HUVECs in a concentration-dependent manner, with 100 nM being the lowest concentration that elicited a significant effect **(Appendix Figure S5A, B)**. Comparative analysis with Bevacizumab revealed similar inhibitory effects, with EC50 values of 0.130 μM for Bevacizumab and 0.083 μM for apelin-dm, respectively **(Appendix Figure S5C)**. Previously, Bevacizumab was shown to exhibit inhibitory effects at concentrations around 100 nM, both in vitro and in CAM assays (Ljoki *et al*, 2022; Ademi *et al*, 2021), suggesting a similar anti-angiogenic effect for apelin-dm and Bevacizumab at this concentration. In the presence of apelin, HUVECs formed a network of capillary-like tubes, evidenced by a significant increase in the number of junctions and tube length, and this effect was counteracted by apelin-dm **(Appendix Figure S6A, B)**. In addition, we found that apelin-dm inhibited both HUVEC and SMC proliferation and migration, especially those

induced by apelin-13 or apelin-36 **(Appendix Figure S6C-E)**. Real-time PCR showed expression of apelin and its receptor in SMCs and HUVECs **(Appendix Figure S6F)**. Analysis of the apelin receptor at the protein level revealed its high expression in HUVEC cells compared to CT-26 and MC-38 cells **(Appendix Figure S6G)**. Further analysis revealed high expression of Furin in SMCs (5193 copies/cell) and HUVECs (6013 copies/cell), while it was lower in cancer cells, with 3667 and 3713 copies/cell for CT-26 and MC-38, respectively **(Fig. 3C)**.

Angiogenesis is a complex intercellular process involving the organization of various cells. To evaluate the effect of apelin-dm in the context of whole tissue, we performed the aortic ring assay **(Appendix Figure S6H, I)**. While apelin induced sprouting of vessel-like structures in the aortic ring assay, apelin-dm repressed this effect. We examined whether apelin-dm could interfere with VEGF-induced angiogenic sprouting in endothelial cells. Our findings indicate that apelin-dm prevents sprouting in endothelial cells caused by VEGF throughout the treatment periods **(Appendix Figure S6J, K)**. Under these conditions, apelin-dm was comparable in effect to Bevacizumab. We also tested the anti-angiogenic effect of apelin-dm using the chick chorioallantoic membrane (CAM) assay **(Fig. 3D, E)**. Apelin-dm treatment impaired both basal CAM angiogenesis and CAM angiogenesis induced by apelin. Examination of the CAM vasculature by isolectin B4 staining showed that while apelin induced vessel formation, apelin-dm mainly affected the formation of small vessels **(Fig. 3D, E,** yellow arrows**,** and **Appendix Figure S7A)**. Additionally, we used the neonatal mouse retinal model as an in vivo assay to examine the effect of apelin-dm on neoangiogenesis. At birth, the retina is avascular, and a superficial vascular plexus grows from the center to the periphery during the first week after birth (Selvam *et al*, 2018). Isolectin B4 staining of the retinal vasculature at P5 revealed that apelin administration significantly increased vascular sprouting in mice compared to controls **(Fig. 3F, G)**. In both untreated and apelin-treated mice, sprouting vessels were reduced by apelin-dm administration. Additionally, apelin-dm hindered VEGF-induced endothelial cell sprouting, and disrupted angiogenesis in the CAM assay **(Fig. 3H, I** and **Appendix Figure S7B)**.

To investigate the mechanism by which apelin-dm represses VEGF-induced angiogenesis, we first analyzed its effect on HUVEC proliferation and migration in response to VEGF. As depicted in **Fig. 3J, K**, while VEGF significantly promoted HUVEC proliferation and migration, the presence of apelin-dm suppressed these effects. Furthermore, analysis of ERK activation, a signaling pathway mediated by VEGF and involved in HUVEC proliferation and migration, showed that while VEGF induced ERK activation, treatment with apelin-dm attenuated this effect **(Fig. 3M, N)**. This suggests that apelin-dm interferes with the VEGF signaling pathway, which may explain the reduced angiogenesis mediated by VEGF in the presence of apelin-dm.

In soft-agar assays, apelin-dm significantly inhibited the clonogenicity of colon cancer cells, countering the apelin-induced increase in colony formation **(Fig. 3L, O)**. Apelin-13 and apelin-36 stimulated cancer cell migration, while apelin-dm mitigated this effect, suggesting interference with apelin's autocrine action **(Fig. 3P** and **Appendix Figure S8)**. Indeed, all the analyzed colon cancer cells express both apelin and the apelin receptor **(Appendix Figure S2B)**.

f

Computational docking analysis of apelin peptides and apelin-dm with apelin receptor: Predicting binding modes and affinity

Aligning apelin-13 with the experimental structure of the AMG3054 peptide mimetic in the presence of the active apelin receptor cryo-EM structure suggests that the C-terminal region of apelin-13 inserts into a deep pocket **(Fig. 3Q)**. Additional CABS-flex simulations induced minor changes in the N-terminal region of apelin-13, while the C-terminus remained deeply anchored compared to the starting position of the peptide. Apelin-dm, apelin-36, and apelin-17, docked using CABS-dock, wrapped around the apelin receptor, showing additional favorable interactions in the peptide C-terminal region compared to apelin-13, particularly for apelin-dm and apelin-36. Models of the apelin receptor with apelin-dm exhibited higher total binding energy values than

models with apelin-13 or apelin-17, indicating superior binding of apelin-dm. The predicted binding energy values between apelin-36 or apelin-dm and the receptor were similar **(Fig. 3R)**. APOP identified allosteric sites, with the top site matching the peptide-binding site in the C-terminal region (allosteric site 1) **(Fig. 3Q)**. Another allosteric site, accessible to apelin-13, apelin-17, apelin-36, and apelin-dm, was identified and labeled allosteric site 2. A third allosteric pocket (allosteric site 3) can also interact with the N-terminal region of apelin-36 or apelin-dm **(Fig. 3Q)**. The predicted binding energy scores favored apelin-dm or apelin-36 over apelin-13 or apelin-17 **(Fig. 3R)**.

Apelin-dm peptide-driven changes in apelin receptor conformation

Apelin and apelin-dm's effects on apelin receptor affinity and conformation were assessed using plasmon waveguide resonance (PWR) (Soulet *et al*, 2020). The sensor, pretreated with polylysine, captured cell fragments through electrostatic interactions. After capturing fragments, ligand incrementation induced spectral changes tracked for both polarizations. Ligand affinity analyses showed apelin-dm's highest affinity (KD approximately 30 pM) for cell membrane fragments, surpassing apelin (KD approximately 100 pM) **(Fig. 3S-U)**. Spectral changes under ligand binding revealed distinct conformational changes induced by apelin-dm and apelin-13, with apelin-dm causing more substantial and anisotropic shifts **(Fig. 3V)**. These differences indicated ligand-induced distinct receptor conformational states. Notably, using membranes from HEK cells lacking apelin receptor under the same conditions did not induce significant conformational changes in the receptor **(Appendix Figure S9)**.

Apelin-dm exhibits high-affinity competition with apelin for apelin receptor binding.

The ability of apelin-dm to repress various biological functions of apelin suggests that apelin-dm probably acts as an inhibitor of endogenous and exogenous apelin in terms of receptor binding. Previously, apelin was reported to cause clathrin-mediated apelin receptor internalization (He *et*

al, 2016; Reaux *et al*, 2001; El Messari *et al*, 2004a) and translocation of β-arrestin to the cell surface, indicating translocation to the phosphorylated apelin receptor (Lee *et al*, 2010). After apelin-induced internalization, the apelin receptor can either be recycled to the cell surface or be degraded in lysosomes (Lee *et al*, 2010). Therefore, we compared the effects of apelin and apelin-dm on the cellular recycling of the apelin receptor. To facilitate the functional analysis of receptor internalization, we used U2OS cells stably co-expressing the human apelin receptor and β-arrestin 2-GFP. Stimulation of these cells with Tamara-apelin for 30 minutes induced receptor internalization, as visualized by the appearance of a punctuated pattern of red (Tamara-apelin) and green (apelin receptor/arrestin 2-GFP) fluorescence **(Fig. 4A)**. In contrast, cells treated with apelin-dm showed reduced Tamara-apelin receptor internalization **(Fig. 4A)**. The use of the same cells revealed that apelin-dm, like apelin, induces receptor internalization that colocalizes with clathrin **(Fig. 4B)**. Similar to apelin, apelin-dm dose-dependently increases the Bioluminescence Resonance Energy Transfer (BRET) signal between the apelin receptor and Rab5, confirming the ability of both apelin and apelin-dm to promote apelin receptor internalization **(Appendix Figure S10A)**. Using HEK293A cells stably expressing apelin receptor-EGFP fusion protein, we found that six hours after apelin-13 washout, the apelin receptor seemed to be mainly returned to the cell surface. In contrast, in cells treated with apelin-dm, the intracellular vesicles of the apelin receptor remained internalized **(Appendix Figure S10B)**, suggesting delayed or blocked recycling of the apelin receptor in the presence of apelin-dm. To further validate that apelin-dm functions by directly competing with apelin for receptor binding, competitive binding assays were performed to verify the binding affinities of the radiolabeled peptide, [125I]-(Pyr1)-apelin-13, in the presence of apelin-13 and apelin-dm. As shown in **Fig. 4C**, both peptides potently inhibited the specific binding of the [125I]-(Pyr1)-apelin-13 peptide to the apelin receptor in a concentration-dependent manner. However, the apelin-dm peptide showed an IC50 about 2.5 times smaller than that of apelin-13 (0.45 nM versus 1.13 nM), suggesting that lower concentrations of apelin-dm are required to compete with apelin-13 for apelin receptor binding.

These results indicate that apelin-dm competes with apelin for apelin receptor binding and represses its activation and internalization.

Apelin-dm modulates Elabela activity and its receptor binding

Alongside apelin, Elabela can activate the apelin receptor, boasting a distinct amino acid sequence from apelin (Read *et al*, 2019). It colocalizes with apelin in endothelial cells and circulates in plasma. Elabela shares functional roles with apelin in angiogenesis and cancer (Yang *et al*, 2017). To investigate whether apelin-dm affects the interaction between Elabela and the apelin receptor, we conducted PWR and ligand affinity analyses. Our findings showed that apelin-dm competes with Elabela's binding to the apelin receptor, as evidenced by an increased KD from 27 ± 1 to 56.6 ± 2.6 in the presence of apelin-dm **(Fig. 4D)**. Additionally, ERK activation analysis in HEK-apelin receptor cells revealed that apelin-dm inhibited Elabela-induced ERK activation **(Fig. 4E)**. These results suggest that apelin-dm competes with apelin and Elabela for the apelin receptor and influences their functions.

Apelin-dm targets apelin and non apelin-related signaling pathways

To evaluate the impact of apelin-dm on apelin receptor downstream signaling, we initially explored its potential effect on the ERK and AKTpathways, known to be activated by apelin (Masri *et al*, 2004). Our findings revealed that while apelin treatment activated ERK and AKT in HUVECs, SMCs, CT-26 cells, and HEK 293 cells, apelin-dm significantly inhibited these processes **(Fig. 4F, G** and **Appendix Figure S11)**. For a more comprehensive assessment of the effect of apelin-dm on various kinase activities, we conducted a screening of diverse kinase activities using the PamGene technology (Versele *et al*, 2009) that showed substantial differences in kinase activity profiles in control and treated cells. Apelin treatment affected phosphorylation in 60 PTK and 58 STK peptides, whereas apelin-dm induced lower changes in

phosphorylation in 15 PTK and 37 STK peptides **(Fig. 4H-K** and **Appendix Figure S12)**. Additionally, 22 PTK and seven STK peptides exhibited significantly dysregulated phosphorylation between apelin and apelin-dm-treated cells. Apelin treatment indicated significantly higher activity for Src family kinases (Src, Lyn, Lck, HCK, BLK, Fyn) and insulin receptor family (InsR, IRR) among PTKs, as well as heightened activity in the ERK (ERK1 and ERK2) and CDK (CDK11, CDK9) families within STKs **(Fig. 4L, M** and **Appendix Figures S13-15)**. Conversely, in apelin-dm-treated cells, Src family kinases (Lyn, Lck, HCK, BLK) and CDK family (CDK11, CDK9) exhibited weaker activity compared to apelin-treated cells, indicating repression by apelin-dm. Mean kinase statistics and mean kinase scores for branches and nodes in the phylogenetic tree of the human protein kinase family were also calculated. Additionally, the top upstream kinases from the significantly altered PTK/STK peptides by apelin-dm were predicted **(Appendix Figure S15A-C)**.

Therapeutic efficacy of apelin-dm peptide

To assess the tumor-suppressive potential of apelin-dm, mice with subcutaneously injected CT-26 and MC-38 cells were treated intraperitoneally with apelin-dm (30 mg/kg), apelin receptor antagonist ML221 or a saline vehicle control **(Fig. 5A)**. Tumor growth, apoptosis, proliferation, and/or the angiogenic index of the developed tumors were first evaluated. Apelin-dm treatment significantly reduced tumor growth compared to controls, as observed in daily monitored tumor volumes for both mice tumor models **(Fig. 5B, C)**. The anti-tumor effect of apelin-dm was comparable to the effect of the apelin receptor antagonist ML221 **(Fig. 5D)**. The CD31 and KI-67 staining of tumor sections revealed decreased angiogenic **(Fig. 5E, H, I, J)** and proliferative indices **(Fig. 5F, H, K, L)** in apelin-dm-treated mice inoculated by CT-26 and MC-38 tumor cells, respectively. Immunohistochemistry analysis showed increased pro-apoptotic protein BIM levels in apelin-dm-treated mice tumors **(Fig. 5G, M, N)**, indicating enhanced cell death**.** Co-staining for KI-67 and CD31 in CT-26 and MC-38 tumors **(Fig. 5H)** derived from apelin-dm-

treatd mice showed that the reduced KI-67 staining was predominantly observed in the cancer cells within the tumors. Apelin-dm also attenuated tumor growth **(Fig. 5O, P)** and angiogenesis **(Fig. 5O, Q)** induced by cancer cells in the CAM assay, and reduced tumor blood flow in mice with subcutaneous HCT116 colon cancer tumors **(Fig. 5R, S)** and other cancer cell types (MDA-MB-231) **(Fig. 5T)**. Apelin-dm's anti-angiogenic and anti-tumorigenic activity was comparable to bevacizumab, and no obvious toxicity in treated mice was observed **(Appendix Figure S16)**.

Apelin-dm peptide represses early event of colorectal liver metastasis

In liver colorectal metastasis, metastatic cancer cells trigger the adhesion molecule E-selectin expression in liver endothelial cells, facilitating tumor cell arrest and metastasis (Scamuffa *et al*, 2008; Buccafusca *et al*, 2019). We investigated apelin's role by exposing human hepatic endothelial cells (LSEC) to 100 nM apelin **(Fig. 6A)**. E-selectin mRNA levels increased at 2 hours, peaked at 6 hours, and remained elevated even after 8 hours of apelin treatment. At the protein level, E-selectin expression peaked at 24 hours, followed by a decrease at 32 hours **(Fig. 6B)**. Apelin also induced E-selectin expression in endothelial cells HMEC-1 and HUVEC **(Fig. 6C, D)**. However, the dynamics of apelin's effect differed in these endothelial cells compared to LSECs. While E-selectin expression initially increased after 2 hours of incubation with apelin, it subsequently declined but remained elevated compared to baseline levels after 6 hours. This divergence may arise from inherent variations in the regulatory mechanisms governing E-selectin expression, suggesting potential differences in the regulatory pathways and signaling mechanisms among these cell types in response to apelin. Apelin-dm peptide inhibited apelin-induced E-selectin, as did the apelin receptor antagonist MM54 in LSECs (**Fig. 6E, F)**. The effect of apelin-dm on E-selectin induction was also assessed in mice intrasplenically/portal-inoculated with CT-26 cells. While, liver colonillizing CT-26 cells induced E-selectin expression, apelin-dm significantly repressed hepatic E-selectin **(Fig. 6G, H)**. MM54 also repressed E-selectin induction mediatd by cancer cells **(Fig. 6I)**. Apelin-dm and MM54-treated

groups exhibited reduced hepatic metastases formation two weeks post-treatment **(Fig. 6J, K)**. Taken together, these results highlight apelin's role in liver colonization and apelin-dm's ability to repress these processes **(Fig. 7)**.

Pharmacological profile of apelin-dm peptide

The apelin-dm peptide's pharmacological profile was assessed, starting with acute toxicity in Balb/C mice (50-1000 mg/kg, no adverse effects). The maximum tolerated dose (MTD) was >1000 mg/kg intraperitoneally **(Fig. 8, Appendix pharmacological study 1)**. Repeated administrations (300 mg/kg/day for 14 days) showed safety through hematology, blood chemistry, and histological analyses **(Fig. 8, Appendix pharmacological study 2)**. In vivo stability was tested, revealing rapid systemic circulation and detection in serum (0.65 ± 0.3 µM at 5 and 10 min) with a half-life of 20 min **(Fig. 8, Appendix pharmacological study 3)**. In-solution properties showed 54% and 26% protein binding for human and mouse plasma, solubility of 187.3µM in PBS at 2.10-4M, and a half-life of 1121 min (>18 h) in human plasma **(Fig. 8, Appendix pharmacological study 4)**. Intrinsic clearance in liver microsomes was <115.5µL/min/mg **(Fig. 8, Appendix pharmacological study 4)**. Of the 16 CYP isoforms tested, apelin-dm inhibited CYP3A4 and induced 10.9%, 5.2%, and 5.0% inhibition in the hERG cardiac toxicity assay at concentrations of 10-5M, 10-6M, and 10-7M, respectively **(Fig. 8, Appendix pharmacological study 4)**. When compared to various reference compounds, used at the clinical setting in all these assays, apelin-dm emerges as a safe, stable, and specific potential drug candidate overall.

Discussion

Metastasis stands as a primary contributor to mortality among patients grappling with diverse cancer types, notably colon cancer (Morgan *et al*, 2023; Buccafusca *et al*, 2019). The insidious dissemination of colon cancer can manifest in both the advanced stages of cancer progression and the pre-invasive phases, influenced by a spectrum of systemic factors secreted by the tumor or its microenvironment (Morgan *et al*, 2023; Buccafusca *et al*, 2019; Wang *et al*, 2023). Apelin, an emerging systemic factor, assumes a pivotal role in tumor advancement, angiogenesis, and the establishment of a premetastatic niche in potential metastatic organs through its intricate interaction with apelin receptor (Feng *et al*, 2016). Consequently, the early identification and prevention of metastasis, whether through traditional treatments or interventions in the apelin/apelin receptor interaction, emerge as crucial strategies in mitigating cancer-related pathologies and fatalities. Within this study, we discerned apelin as a distinctive substrate of Furin, exhibiting resistance to cleavage by other proprotein convertases (PCs). Our findings furnish a mechanistic understanding of the anti-tumorigenic, anti-metastatic, and anti-angiogenic effects attributed to apelin-dm, which arises from targeted modulation of the Furin cleavage site in the apelin precursor.

The dysregulation of apelin and its receptor, marked by overexpression and aberrant activation, plays a pivotal role in the onset and progression of numerous human malignancies, leading to reduced survival rates and compromised therapy sensitivity (Feng *et al*, 2016; Gourgue *et al*, 2020; Zuurbier *et al*, 2017; Bernier-Latmani *et al*, 2022; Berta *et al*, 2010; Cazzato *et al*, 2015). In our study, we observed the co-expression of apelin and its receptor in both primary and metastatic tissues of colon cancer patients. This observation indicates that colon tumors sustain the capability to produce apelin and remain responsive not only in primary tumors, as previously reported (Picault *et al*, 2014a), but also across various stages of tumor progression, including metastasis. This suggests that the autocrine loops mediated by apelin play a pivotal role not only

in the growth and survival of primary tumors but also in facilitating the metastatic dissemination of cancer cells and angiogenesis. Previous studies have reported the expression of apelin and its receptor in endothelial cells (del Toro *et al*, 2010), smooth muscle cells (SMC) (Pitkin *et al*, 2010), and cancer cells (Williams *et al*, 2024). Comparative analysis of these protein expressions revealed higher levels of apelin and its receptor in endothelial and SMC cells compared to cancer cells. Similarly, Furin expression was also found to be higher in endothelial and SMC cells compared to CT-26 and MC-38 cancer cells. We also found that, like apelin, Furin is induced by hypoxia in endothelial cells.

Upon activation, apelin receptor triggers various pathways crucial to the growth, survival, and migration of both cancer and endothelial cells (Read *et al*, 2019; Falcão-Pires *et al*, 2010; Picault *et al*, 2014b). Consequently, our focus in this study centered on unraveling the impact of apelin-dm on these critical processes within colon cancer and endothelial cells. Through a series of in vitro and in vivo models simulating tumor progression and colorectal liver metastasis via intrasplenic injection of colon CT-26 and MC-38 cancer cells expressing apelin-dm, we unearthed compelling evidence of the anti-cancer and anti-angiogenic properties of apelin-dm. Notably, similar effects were replicated using purified apelin-dm peptide. This peptide not only hindered angiogenesis driven by apelin but also curtailed VEGF-stimulated angiogenesis by repressing VEGF-induced proliferation, migration, and signaling pathways. Additionally, apelin and apelin receptor expression was reported to be increased in endothelial and non-endothelial cells following VEGF stimulation(Kojima & Quertermous, 2008; Takano *et al*, 2018), suggesting VEGF's involvement in the enhanced autocrine action of apelin in endothelial cells. This implies that apelin-dm can repress VEGF-induced proliferation and migration through this autocrine action. We also found that apelin-dm interferes with the interaction between Elabela and the apelin receptor and represses Elabela-induced receptor activation. Apelin-dm exhibited also a pronounced inhibitory effect on colony formation and migration of colon cancer cells,

endothelial cells, and smooth muscle cells. These observations provide plausible mechanistic insights into how this inhibitor may effectively impede tumor growth and angiogenesis.

Our investigation unveiled that the inhibition of proapelin processing appears to heighten the affinity of the apelin receptor for apelin-dm. This observation was substantiated through comprehensive docking computations and structural analyses, which were further validated by radioligand binding assays. Constructing the apelin-dm-apelin receptor complex based on the X-ray structure of the apelin receptor-apelin peptide mimetic AMG3054 revealed a distinctive wrapping of apelin-dm (or apelin-36) around the apelin receptor, with a notable concentration of major binding energy in the C-terminal region of the peptide, particularly at the last Phe residue. Intriguingly, the residues cleaved by Furin exhibited a tendency to point away from the receptor, forming limited contact points with the protein. The predicted binding scores, favoring apelin-dm (and apelin-36) over the shorter apelin-13, aligned with experimental data, supporting the additional favorable contacts for the longer 36-residue peptides. The predicted interaction energy values are relatively similar between apelin-36 and apelin-dm, but apelin-dm is more stable and not cleaved as compared to the wild-type apelin-36, which is rapidly cleaved upon synthesis. This allows for major competition on the apelin receptor to occur between mature apelin rather than apelin-36. The binding pocket crucial for interaction with the C-terminal region of apelin was predicted to be allosteric, corroborating with observed flexibility and structural changes in this region of the receptor. While apelin-13 was predicted to engage two allosteric sites, apelin-dm (or apelin-36) was anticipated to establish further contacts with an additional allosteric site situated on the receptor's side. This suggests the possibility that the two peptides (e.g., apelin-13 and apelin-dm) induce slightly different structural changes upon binding. The precise 3D predictions of such changes remain challenging, acknowledging the inherent flexibility of the N-terminal of apelin-dm, yet the overall position of the peptides on the apelin receptor seems reasonable. It is important to note that the exact high atomic resolution of apelin-dm remains

unknown. Utilizing a plasmon waveguide resonance (PWR) assay, we discerned that apelin-dm and apelin-13 elicited distinct conformational changes in the receptor, indicative of potential differences in apelin receptor affinity and in the likely interactions with the predicted allosteric sites for apelin-13 versus apelin-dm.

Furthermore, our findings unveiled that, while apelin triggered the phosphorylation of various kinases associated with cell proliferation, survival, and migration encompassing members of the Src, InsR, ERK, and CDK family kinases, apelin-dm exhibited a diminished effect. Notably, apelin-dm not only attenuated the stimulatory effects of apelin but also inhibited the ability of apelin to induce various kinase activities. This divergence in kinase activation profiles further emphasizes distinct functional impact of apelin-dm compared to its processed peptide apelin-13.

Protein half-life exhibits significant variability spanning several orders of magnitude, (Toyama & Hetzer, 2013) with longer-lived proteins typically serving as 'housekeeping' proteins, while shorter-lived proteins often function as phosphorylation targets and signaling molecules. Apelin, a key player in physiological processes, has a notably short in vivo half-life (< 5 minutes) (Vickers *et al*, 2002), implicating its rapid turnover and degradation. Initial studies proposed the involvement of metalloproteases, specifically angiotensin-converting enzyme II (ACE2) and proline carboxy peptidase (PRCP), in apelin degradation, particularly targeting the Pro12-Phe13 residues (Kehoe *et al*, 2016). ACE2, in particular, efficiently hydrolyzes apelin-13, and apelin-36 (Vickers *et al*, 2002). Interestingly, the generated fragments from ACE2 cleavage did not induce apelin receptor internalization in vitro, suggesting that these cleavages may induce a distinct conformational state of the apelin receptor compared to full-length peptides (El Messari *et al*, 2004b). Another identified cleavage site between Leu5-Ser6 residues was attributed to neprilysin (NEP) (McKinnie *et al*, 2016). Our study revealed that modifying the cleavage site of the apelin precursor significantly increased its half-life. This implies that potential conformational changes

introduced by cleavage site mutations may prevent the degradation of apelin-dm by proteases such as ACE2 and NEP. Ligand-receptor dynamics often involve trafficking to lysosomes upon binding, where the ligand is released and degraded while the receptor undergoes recycling or complex degradation (Bonecchi *et al*, 2008). The extended half-life of certain receptors, previously associated with 'slow' recycling between endosomes and the cell surface, has been reported for various receptors, including decoy receptors and membrane-localized vascular endothelial growth factor receptor-1 (mVEGFR1) (Boucher *et al*, 2017). The stability and trafficking of mVEGFR1 are regulated by the palmitoylating enzyme DHHC3 and depalmitoylating enzyme APT1. Impaired mVEGFR1 palmitoylation results in increased trafficking to lysosomes for degradation, disrupting vascular morphogenesis (38). Our findings highlight the impact of ligand half-life in delaying receptor recycling and trafficking upon binding, subsequently altering receptor function and leading to reduced angiogenesis and tumor progression.

Our investigation into the pharmacokinetic properties of apelin-dm, which revealed approximately 50% plasma protein binding, presents several advantages that warrant consideration in therapeutic contexts. These binding properties strike a balance between a rapid onset of action and a prolonged duration of therapeutic effect. While a portion of the drug is bound to plasma proteins, ensuring a reservoir for sustained release, an equally substantial fraction remains unbound and pharmacologically active. This equilibrium allows for the swift attainment of therapeutic concentrations in the bloodstream while maintaining a steady supply of bioavailable drug molecules over an extended period. Consequently, apelin-dm may offer a favorable pharmacokinetic profile suitable for conditions requiring both immediate intervention and sustained therapeutic coverage. Highly protein-bound drugs may be susceptible to drug interactions and alterations in pharmacokinetics due to competition for plasma protein binding sites, potentially leading to suboptimal therapeutic outcomes or an increased risk of toxicity.

Conversely, drugs with minimal protein binding may exhibit rapid clearance and reduced bioavailability, necessitating frequent dosing regimens or higher doses to maintain therapeutic efficacy. Apelin-dm's 50% plasma protein binding confers a degree of flexibility, striking a harmonious balance between efficacy and safety, and minimizing the likelihood of pharmacokinetic fluctuations that could compromise treatment efficacy. Previously, peptides with similar properties have been well tolerated with few side effects, suggesting that apelin-dm is likely to be translatable into clinical practice (Davenport *et al*, 2020).

We elucidate the crucial role of apelin precursor cleavage by Furin and identify apelin-dm as a peptide with anti-tumorigenic and anti-metastatic functions. Importantly, this peptide exhibits favorable pharmacological profiles. Overall, we present apelin-dm as a potent, selective, non-toxic inhibitor of the apelin receptor interaction, demonstrating efficacy in a mouse model of colon cancer and colorectal liver metastasis. Our data strongly support apelin-dm as a promising lead compound for further exploration in medicinal chemistry and drug development.

Materials and Methods

Reagents and Tools

Reagent/Resource	Reference or Source	Identifier or Catalog Number
Experimental Models		
Human Peripheral Blood Mononuclear Cells (hPBMCs)	Institute Bergonié, Bordeaux or EFS, Bordeaux	NA
Colorectal cancer patients' sample	Institute Bergonié, Bordeaux	NA
HT29 cells (H. sapiens)	ATCC	HTB-38
LoVo cells (H. sapiens)	ATCC	CCL-229
HEK-293 cells (H. sapiens)	ATCC	CRL-1573
U2OS cells (H. sapiens)	ATCC	HTB-96
MDA-MB-231 cells (H. sapiens)	ATCC	HTB-26
MC38 cells (M. musculus	Kerafast	CVCL_B288
CT26 cells (M. musculus	ATCC	CRL-2638
CHO-FD11 cells (C. griseus)	Gordon et al, 1997	NA
C57BL6/J (M. musculus)	Charles Rivers Laboratories	N/A
Rag2/γc (M. musculus)	The Jackson Lab	NA
BALB/c (M. musculus)	Charles Rivers Laboratories	NA
Recombinant DNA		
pIRES-APLN	This study	NA
pIRES-APLN-V5	This study	NA
pIRES- APLN	This study	NA
pIRES-apelin-dm	This study	NA
APLNR-pEGFP-N1	This study	NA
Antibodies		
anti-apelin	Eurogentec	NA

anti-apelin receptor	Abcam	ab84296
Anti-Ki67	Cell Signaling	9129T
Anti-c-caspase 3	Cell Signaling	96617
anti-CD31	BD PharmingenTM	553370
anti-phospho ERK	Cell Signaling	9106S
anti-ERK	Cell Signaling	4695
anti-β-actin	Cell Signaling	4967
Anti–E-selectin	Abcam	ab2497
Anti- human Clathrin	abcam	ab2731
Anti-V5	Invitrogen	NA
Secondary anti-rabbit	Cell Signaling	7074
Secondary anti-mouse	Cell Signaling	7076
Oligonucleotides and other sequence-based reagents		
PCR primers	This study	Appendix Methods
Chemicals, Enzymes and other reagents		
apelin peptides	Clinisciences	NA
pERTKR-AMC Fluorogenic Peptide Substrate	R&D system	ES013
M-PER lysis buffer	Thermo Fisher Scientific	78503
Halt Protease and Phosphatase inhibitors	Thermo Fisher Scientific	87786 and 78420
STK reagent kit	PamGene	32201
PTK reagent kit	PamGene	32112
Bovine serum albumin (BSA)	Euromedex	04-100-812-C
[125I]-MIP-3b	Perkin Elmer	NA
MIP-3b	R&D Systems	361MI
FITC Annexin V Apoptosis Detection Kit I	BD Pharmingen™	NA

Software		
Protein identification	Proteome Discoverer 1.4 Mascot 2.5	NA
	Sequest HT	NA
	Percolator algorithm	NA
Software Docking	CABS-dock flexible docking engine	Kurcinski *et al*, 2019
	PULCHRA	Rotkiewicz & Skolnick, 2008).
	MMTK	http://dirac.cnrs-orleans.fr/MMTK.html
	pyDockEneRes [65]	Romero-Durana *et al*, 2020
	PPM server	Lomize *et al*, 2012
	APOP	Kumar et al, 2023
	Fpocket	Le Guilloux *et al*, 2009
	UCSF ChimeraX [69]	Pettersen *et al*, 2021
	PyMOL	https://www.schrodinger.com
ImageJ/Fiji	https://imagej.nih.gov/ij	NA
BioNavigator V63	PamGene	BN63
Other		
BD AccuriTM C6 Cytometer		
Nikon C2si Eclipse Ti-S		
Tecan Infinite® F200 PRO, Tecan Group Ltd.		

Methods and Protocols

Patient samples

Samples from 35 colorectal cancer patients, along with corresponding liver metastatic tissues and adjacent normal regions, were collected from frozen and formalin-fixed paraffin-

embedded (FFPE) tissues. The specimens were clinically and histopathologically diagnosed at Institut Bergonié, Bordeaux. The tissues, acquired after resection, were promptly placed on ice post-surgery and snap-frozen in liquid nitrogen for subsequent analysis. All human specimens were obtained following written informed consent approved by Bergonié Institute, Bordeaux, France. Patient consent forms for all samples were obtained at the time of tissue acquisition. Biopsies were de-identified.

Analysis of public datasets

The comparison between colon tumor and normal tissues regarding *GSN, Spg20, NSUN5, APLN, APLNR* mRNA expression was performed using GEPIA (Tang *et al*, 2017). The correlation between CYR6, APLN, and APLNR mRNA expression, and RIC8A, APLN, and APLNR mRNA expression in colon adenocarcinoma (COAD) was also determined using GEPIA (Tang *et al*, 2017).

Cloning and mutagenesis

pIRES-APLN and pIRES-APLN-V5 constructs were generated by amplifying the coding region of human apelin by PCR using specific primers **(Appendix Methods)**. Mutagenesis was carried out by an oligonucleotide-directed mutagenesis system (Quick Change site-directed mutagenesis kit, Stratagene) according to the manufacturer's recommendation using pIRES- APLN construct. The oligonucleotides used to generate the mutations for pIRES-apelin-dm generation are listed in **Appendix Methods**. Apelin cDNA from human colorectal cancer tissue was amplified using PCR and specific primers and the PCR product was subcloned into the pEGFP-N1 vector to generate the APLNR-pEGFP-N1 vector. All constructs were verified by sequencing.

Cell transfection, transduction and culture

LoVo, HT-29, CT-26, MC-38, U2OS, and MDA-MB-231 cells were procured from ATCC (Manassas, VA, USA). CHO-FD11 cells with reduced Furin activity were characterized previously (Gordon *et al*, 1997). All cells were maintained in modified Eagle's medium (MEM), Dulbecco's modified Eagle's medium (DMEM) or RPMI-1640 with 10% fetal calf serum, 100 units/ml penicillin, 100 µg/ml streptomycin, and 2mM L-Glutamine (Dutscher), and incubated at 37 °C with 5% CO2. Authenticity and mycoplasma screening were routinely performed by PCR (every two weeks and before each animal experiment for mycoplasma screening). For hypoxic experiments, endothelial cells were serum-starved and placed in a sealed, humidified chamber maintained at 1% O_2 and 5% CO_2 for different time periods ranging from 4 hours to 24 hours. Transfections used Effectene transfection reagent (Qiagen, Germany). Lentiviral vectors with wild-type apelin or apelin-dm cDNA were prepared using pIRES plasmids, cloned into a self-inactivating lentiviral vector with a tdTomato reporter gene (pRRLsin-MND-hPGK-tdTomato-WPRE) under myeloproliferative sarcoma virus enhancer control. All constructs were sequenced, and lentiviral vector production was conducted by the "Vect'UB" service platform at the TMB-Core of the University of Bordeaux.

Ribonucleic acid (RNA) extraction, real time PCR and droplet digita PCR (ddPCR)

For real time PCR, total RNA was extracted using an RNA isolation kit (Macherey-Nagel) including DNase treatment (Qiagen), according to the manufacturer's instructions, and qPCR data were acquired with the StepOnePlusTM Real-Time PCR System (Applied Biosystems, Courtaboeuf, France), as previously described (Scamuffa *et al*, 2008). For ddPCR, cDNA was synthesized from 2 µg of total RNA using Maxima Reverse Transcriptase (Fisher Scientific), primed with oligo-dT primers (Fisher Scientific) and random primers (Fisher Scientific). ddPCR was performed as described in the Appendix Methods.

Production of apelin-13, apelin-36 and apelin-dm peptides.

Peptides apelin-36 (LVQPRGSRNGPGPWQGGRRKFRRQRPRLSHKGPMPF), apelin-13 (QRPRLSHKGPMPF) and apelin-dm (LVQPRGSRNGPGPWQGGGSSKFSSQRPRLSHKGPMPF) were synthesized by Neo Biotech (Clinisciences, France) and resuspended in water or PBS to a 1-5 mM working solution. Peptides were added directly into the medium of the cells or injected into mice and fertilized eggs for the chick chorioallantoic membrane assay at the indicated concentrations.

Immunoblotting

Western blot analysis was conducted as previously described by Scamuffa et al. (2008), with modifications to detect various apelin isoforms. Proteins were separated using a 13.3% SDS-PAGE acrylamide-glycerol gel, followed by transfer onto a nitrocellulose membrane (Protran 0.2 µm, Amersham). The membrane was fixed with 2.5% glutaraldehyde (Sigma G7651) and probed using HRP-conjugated secondary antibodies (Santa Cruz) (refer to **Appendix: Methods**)

Measurement of PCs activity

PC activity in cells and tissues was assessed by evaluating the ability of the enzymes to digest the Furin substrate, the fluorogenic peptide pERTKR-MCA, as described previously (Sfaxi *et al*, 2014; Scamuffa *et al*, 2014) and in **Appendix Methods** .

Internalization assay

U2OS cells stably co-expressing human apelin receptor and β-arrestin 2-GFP were seeded on poly D-lysine-coated glass slides in 12-well dishes (3×10^5 cells/well). After 12 hours, the medium was replaced with fresh medium containing apelin-(5-carboxytetramethylrhodamine: apelin-13-TAMRA (100 nM) (Proteogenix, Oberhausbergen, France), apelin-dm, or apelin-13-TAMRA and apelin-dm (100 nM) for 45 minutes. In another experiment, these cells were treated with apelin (100 nM) or apelin-dm (100 nM) and stained with mouse anti-human clathrin heavy

chain antibody (Abcam). For washout experiments, cells were incubated for 30 minutes with apelin peptides (100 nM), replaced with serum-free medium, and fixed 2 hours after washout. Analysis was performed using a Zeiss LSM-780 confocal microscope.

Bioluminescence Resonance Energy Transfer (BRET) Measurement

For the BRET assays, phenol red-free medium was removed from HEK293T cells transiently transfected with apelin receptor-Rluc and Rab5-YFP, and replaced with PBS containing calcium and magnesium. The assay was initiated by adding 10 µl of the cell-permeant Renilla luciferase substrate, coelenterazine h, to achieve a final concentration of 5 µM. Five minutes later, apelin and apelin-dm were added to assess their activity. Plate readings were taken 15 minutes after substrate addition. BRET signals were collected using a Mithras LB940 instrument, which integrates signals sequentially in the 465-505 nm and 515-555 nm windows using appropriate bandpass filters, managed by MicroWin 2000 software. Net BRET signals were calculated by subtracting the BRET signal from cells expressing only Rluc-tagged apelin receptor from those co-expressing both Rluc-tagged apelin receptor and YFP-tagged Rab5.

Radioligand binding assay

Radioligand binding assay (Euroscreen catalog: FAST-020B) was performed in 96-well plates (Master Block, Greiner, 786201) containing apelin receptor membrane extracts (2µg protein/well), 0.02 nM [125I]-MIP-3b (Perkin Elmer, custom product) and apelin-13 or apelin-dm at various concentrations. Nonspecific binding was determined using a 200-fold excess of MIP-3b (R&D Systems, 361MI). Dose-response curves were established and the estimated IC_{50} values were calculated for each compound.

Soft agar, proliferation and apoptosis assays

Anchorage-independent colony formation assay was performed as previously described (Sfaxi *et al*, 2014; Scamuffa *et al*, 2014). Proliferation assays were performed using an IncuCyte live-cell microscopy incubator (Essen Bioscience) as previously described (Soulet *et al*, 2020). For the apoptosis assay, tumor cells were grown to 70% confluency, washed repeatedly to remove serum, and then incubated for the indicated time periods in serum-free media. Cells were washed and stained with FITC-labeled Annexin V using the FITC Annexin V Apoptosis Detection Kit I (BD Pharmingen™), according to the manufacturer's instructions. Cells were analyzed by flow cytometry (BD Accuri^{TM} C6 Cytometer), as previously described.(Scamuffa *et al*, 2014)

Tube-like formation assay

HUVECs were seeded at a density of 25 × 10^3 cells/well onto chamber slides (Labtek) previously coated with Geltrex (Gibco) at 37 °C for 30 min to allow polymerization. Appropriate medium-containing vehicles, apelin, apelin-dm or bevacizumab were added at various concentrations. The plates were examined for tube formation under an inverted light microscope at various time points. Photographs of the tubular network in the wells were captured using a digital camera attached to an inverted microscope.

Aortic ring assay

All research animals were housed at the University of Bordeaux in a temperature-controlled environment. All experimental procedures were approved by the Institutional Animal Care and Use Committee, University of Bordeaux, and were conducted under the supervision of trained veterinarian. Six-week-old C57Bl/6 male mice were anesthetized with isoflurane for 5 min before being sacrificed. The descending aorta was isolated, cleared of adventitia, and placed in serum-free Opti-MEM (Gibco) supplemented with 1 × antibiotic/antimycotic (Gibco, 100 × stock solution). Aortas were sectioned into ~25 rings of 0.5 mm (about 15-20 per aorta) thickness and placed in fresh serum-free Opti-MEM with 1 × antibiotic/antimycotic for 1 h at

37°C. The embedded rings were incubated with apelin (100nM), apelin-dm (100nM), Bevacizumab (100 nM), and/or VEGF (30ng/ml). For each ring, the microvessels emerging from the main ring and individual branches arising from them were quantified.

Chick chorioallantoic membrane (CAM) angiogenesis assay

Fertilized eggs were allowed to mature *ex ovo*. A small incision was made in the eggshell on day 3 of development, and seven days later, apelin and/or apelin-dm peptide was added to the CAM tissue (100nM). In other experiments $1x10^6$ control tumor cells or the same cells stably expressing wild-type apelin or apelin-dm were directly allowed to grow on the CAM Tissue. Immunohistology *in toto* was performed for vessel staining. Images of CAM vessels were acquired using a Zeiss Axiophot microscope.

Retina angiogenesis assay.

Postnatal Day 5 (P5) mice were intraperitoneally injected daily for 6 days with apelin (10 mg/kg), apelin-dm (10 mg/kg), or both (10 mg each), via intraperitoneal (IP) injection. Following the treatment period, the mice were humanely euthanized, and their eyes were harvested. The eyes were immediately transferred to 4% paraformaldehyde (PFA) for fixation for 10–15 minutes, after which they were transferred to cold phosphate-buffered saline (PBS) on ice in a Petri dish for dissection. The retinas were carefully isolated and fixed in 4% PFA for 2 hours at room temperature or overnight at 4°C. After fixation, the retinas were blocked and permeabilized in a solution containing 1% bovine serum albumin (BSA) and 0.5% Triton X-100 overnight at 4°C. Subsequently, the retinas were washed three times with a buffer solution composed of 0.5% Triton X-100, 1 mM $CaCl_2$, 1 mM $MgCl_2$, and 1 mM $MnCl_2$ in PBS, pH 6.8. The retinas were then incubated with FITC-labeled Isolectin B4 (1:1000; Vector Laboratories) to label blood vessels. Following staining, the retinas were embedded in Tissue-Tek OCT Compound, and 10-µm cryosections were cut. Confocal immunofluorescence images were acquired with an inverted

Nikon C2si Eclipse Ti-S microscope and analyzed using NIS-Elements AR software (Nikon Instruments Europe B.V.).

Maximal tolerated dose (MTD) and repeated dosing toxicity study

Apelin-dm was administered at the maximum tolerated dose to six groups of BALB/c mice (n=6/group; 3 males, 3 females). The control group received saline, while apelin-dm doses were 200, 500, 1000, 1500, and 2000 mg/kg. A single intraperitoneal injection on day 1 was followed by a 14-day observation period. Parameters monitored included mortality, morbidity, clinical signs, and body weights. At study end, gross pathology and organ necropsy were conducted. For the repeated dosing toxicity study, 40 Balb/C mice (5 males, 5 females/group) were injected 5 days/week for 2 weeks with saline or apelin-dm (50, 150, 300 mg/kg). Evaluations encompassed clinical observations, body weight, food consumption, hematology, blood chemistry, gross pathology, selected organ necropsy, and weight, and histopathology examinations. Comprehensive study details are in **Appendix pharmacological studies-1 and -2**.

The Absorption, Distribution, Metabolism, Excretion (ADME) and Pharmacokinetics (PK) studies

For in-solution property studies, plasma-binding protein assays were performed using the equilibrium dialysis technique, and an aqueous solubility test was performed using a shake flask system. For in vitro metabolism studies, the half-life and intrinsic clearance of the apelin-dm peptide were evaluated in human plasma and human and mouse liver microsomes, respectively. Cytochrome P450 (CYP) inhibition was assayed by fluorimetry using recombinant human CYP. Cardiac toxicity was assessed using the hERG-automated whole-cell patch-clamp technique. For each assay, various reference compounds were used for comparison. Details of the complete study are provided in **Appendix pharmacological studies -3 and -4**.

Preclinical efficacy experiments

C57BL/6, BALB/c, or Rag2/γc mice (6–8 weeks) from the Jackson Laboratory were employed. Tumor growth effects were assessed by injecting $1x10^6$ control or apelin/apelin-dm expressing CT-26/MC-38 cells subcutaneously into BALB/c, Rag2/γc, or C57BL/6 mice. Additional experiments involved injecting $1x10^6$ control CT-26/MC-38/MDA-MB231 cells into BALB/c, C57BL/6, or nude mice, respectively. Apelin-dm treatment (10 mg/kg, i.p.) or saline control commenced when tumors reached ~60 mm3. LASER Doppler imaging assessed total blood flow, with FlowR® Hemodynamics visualization used for analysis. Results were expressed as % relative to pre-treatment tumor blood flow. Experimental liver metastases were induced as previously described (Sfaxi *et al*, 2014; Scamuffa *et al*, 2008)by intrasplenic/portal injection of $1x10^6$ CT-26/MC-38 cells, followed by randomization into treatment (10 mg/kg, i.p.) or saline groups after 5-6 days,.

Immunostaining and confocal microscopy

Sections derived from colon cancer and metastatic liver patients and their corresponding non-cancerous tissues, or from tumors induced in C57BL/6, BALB/c, or Rag2/γ_c mice, were stained with unconjugated antibodies and fluorochrome-associated secondary antibodies. All samples were mounted with Prolong containing DAPI (Invitrogen), and confocal immunofluorescence images were taken using the inverted microscope Nikon C2si Eclipse Ti-S with NIS-ElementsAR software (Nikon Instruments Europe B.V.).

Proteomic analysis

Three independent biological replicates of total protein extracts from control CT26 cells stably expressing apelin and apelin-dm were compared to control CT-26 cells by label-free protein quantification. Proteins were loaded on a 10% acrylamide SDS-PAGE gel and visualized by Colloidal Blue staining. Migration was stopped when the samples had just entered the resolving

gel and the unresolved region of the gel was cut into only one segment. Sample preparation and protein digestion by trypsin and NanoLC-MS/MS analysis were performed as previously described with modification (Henriet *et al*, 2017) and briefly detailes in **Appendix Methods**. Quantitative data were considered for proteins, quantified by a minimum of two unique peptides, a fold change above 2, and a statistical p-value (Welch's t-test) lower than 0.05.

PamGene Kinase assay

Following treatment with apelin an apelin-dm, the cells were washed and lysed in M-PER lysis buffer and PamGene kinase assay and analysis were performed using arrays spotted with distinct 13-amino acid-long peptide substrates with phosphosites (196 for the protein tyrosine kinase (PTK) and 144 for the serine-threonine kinase (STK) arrays), as detailed in **Appendix Methods**. For generating peptide phosphorylation heatmaps and compare the phosphorylation levels across all samples, normalized Log_2 S100 signals were used. Statistical significance was tested using unpaired *t*-tests, and the results are represented by volcano plots generated using BN63 (BN63; PamGene® International, The Netherlands). Peptides with a *P*-value < 0.05 were considered a significant change in the degree of phosphorylation of a peptide in the two groups.

Docking computations and structural analyses

The crystal structure (PDB file 5VBL) of APLNR in complex with apelin peptide mimetics (AMG3054) (Ma *et al*, 2017; Yue *et al*, 2022) was used for the docking of apelin-13, apelin-17, apelin-36 and apelin-dm and the generation of the apelin receptor-apelin-13, apelin receptor-apelin-17, apelin receptor-apelin-36 or apelin receptor-apelin-dm complex. The ten best apelin receptor-apelin-dm models were generated using the standalone version of the CABS-dock flexible docking engine (Kurcinski *et al*, 2019). The analysis is detailed in **Appendix Methods**. The structural analysis was performed using UCSF ChimeraX (Pettersen *et al*, 2021) and the Figures was prepared using PyMOL (https://www.schrodinger.com).

Plasmon waveguide resonance (PWR)

PWR was used to follow apelin receptor conformational changes upon apelin and apelin-dm addition to HEK-apelin receptor cell membrane fragments overexpressing apelin receptor immobilized on the sensor surface. PWR measurements were performed in a homemade instrument functioning at a fixed wavelength of 632 nm and variable incident angle with an angular resolution of about 0.5 millidegrees, as previously described (Soulet *et al*, 2020). The polarization angle of the incident light was 45° to allow both p-polarized (parallel to the incident light and perpendicular to the sensor surface) and s-polarized (perpendicular to the incident light and parallel to the sensor surface) light resonances to be obtained within a single angular scan. The sensor consists of a BK-7 prism coated with silver and silica to support the waveguide. All the measurements were performed at 22°C.

Statistical Analysis

Unless otherwise indicated, data are presented as mean ± sem. A 2-tailed *t* test and 1- or 2-way ANOVA with Tukey's multiple comparisons test were used to analyze the data. Pearson's coefficient was calculated to determine the correlation between normally distributed protein expression in human tumors. Differences between mice groups were analyzed using the Mann–Whitney test in GraphPad Prism (GraphPad Software). The statistical significance level is illustrated with *P* p-values. Statistical *P* was set than 0.05.

Acknowledgements

We thank Vect'UB and One Cell of the TMB-Core of the University of Bordeaux for the lentiviral vector construction and production. This work was supported by Digestive Group (Cancer Institute Bergonié), by the Region Nouvelle Aquitaine and INSERM.

Author contributions

Béatrice Demours: Investigation; Methodology, Conceptualization; Data curation; Formal analysis; Validation;Writing original draft. **Fabienne Soulet**: Investigation; Methodology; Formal analysis. **Jean Descarpentrie**: Investigation; Methodology; Formal analysis; Software. **Maria Casado**: Investigation; Methodology; Formal analysis. **Isabel Galeano-Otero:** Investigation; Methodology; Formal analysis; Validation. **José Sanchez Collado:** Investigation; Methodology; Formal analysis; Software. **Tarik Smani:** Resources; Supervision; Investigation. **Alvaro González:** Investigation; Methodology; Formal analysis. **Isabel Alves:** Investigation; Methodology; Formal analysis. **Fabrice Lalloué**: Investigation; Methodology; Formal analysis. **Bernard Masri:** Investigation; Methodology; Formal analysis. **Estelle Rascol**: Investigation; Methodology; Formal analysis. **Jean-William Dupuy:** Software; Investigation; Methodology. **Cyril Dourthe:** Software; Investigation. **Frédéric Saltel:** Software; Investigation; Methodology. **Anne-Aurélie Raymond:** Software; Investigation; Methodology. **Iker Badiola:** Investigation; Methodology; Formal analysis; Supervision. **Serge Evrard**: Resources; Investigation; Funding acquisition. **Bruno Villoutreix**: Software; Methodology. **Simon Pernot**: Resources; Investigation; Funding acquisition; Supervision. **Géraldine Siegfried**: Project administration; Conceptualization; Resources; Funding acquisition; Data curation; Formal analysis; Validation; Writing review and editing. **Abdel-Majid Khatib**: Project administration; Conceptualization; Resources; Funding acquisition; Data curation; Formal analysis; Validation; Writing review and editing.

Disclosure and competing interests statement

The authors declare no competing interests.

The paper explained

Problem

Colorectal cancer stands as the second leading cause of cancer-related mortality worldwide and ranks third in global cancer diagnoses. Despite the efficacy of surgical resection and adjuvant treatments in early-stage disease, relapse and metastasis remain common and the underlying mechanisms involved in these processes remained elusive. Thus, the discovery of novel efficient regulator may help elucidating the potential mechanisms of colorectal liver metastasis pathway and provide potential therapeutic strategies for colorectal liver metastasis treatment.

Results

We report apelin specific cleavage and activation by Furin as key player in colon cancer and early events of colon cancer and liver cells interaction leading to metastasis. Alteration of apelin cleavage sites generates apelin-dm peptide that effectively represses the malignant and metastatic phenotype of cancer cells and angiogenesis through modulation of apelin receptor dynamics, affinity, internalization, and diverse apelin signaling pathways. Pharmacokinetic and toxicity assessments confirm the specificity, safety, and stability of apelin-dm.

Impact

Through multi-level studies of cell culture, pathological specimens and animal models, we identify the importance of Furin in apelin activity in colon cancer and liver metastasis and apelin-dm peptide as potential therapeutic strategy, paving the way for further clinical exploration.

Data availability

The sequencing data were deposited in the ProteomeXchange consortium via the PRIDE (Perez-Riverol *et al*, 2019) partner repository with the dataset identifier PXD045256. The article and its supplementary information files contain all the additional data supporting the study's findings. The Supporting Data Values file reports the values for every data point represented in the graphs.

References

Ademi H, Shinde DA, Gassmann M, Gerst D, Chaachouay H, Vogel J & Gorr TA (2021) Targeting neovascularization and respiration of tumor grafts grown on chick embryo chorioallantoic membranes. *PLoS One* 16: e0251765

Andersen CU, Hilberg O, Mellemkjær S, Nielsen-Kudsk JE & Simonsen U (2011) Apelin and pulmonary hypertension. *Pulm Circ* 1: 334–346

B M, H L, H M, B K & Y A (2002) Apelin (65-77) activates extracellular signal-regulated kinases via a PTX-sensitive G protein. *Biochemical and biophysical research communications* 290

Basak A, Chen A, Scamuffa N, Mohottalage D, Basak S & Khatib A-M (2010) Blockade of furin activity and furin-induced tumor cells malignant phenotypes by the chemically synthesized human furin prodomain. *Curr Med Chem* 17: 2214–2221

Bernier-Latmani J, Cisarovsky C, Mahfoud S, Ragusa S, Dupanloup I, Barras D, Renevey F, Nassiri S, Anderle P, Squadrito ML, *et al* (2022) Apelin-driven endothelial cell migration sustains intestinal progenitor cells and tumor growth. *Nat Cardiovasc Res* 1: 476–490

Berta J, Kenessey I, Dobos J, Tovari J, Klepetko W, Jan Ankersmit H, Hegedus B, Renyi-Vamos F, Varga J, Lorincz Z, *et al* (2010) Apelin expression in human non-small cell lung cancer: role in angiogenesis and prognosis. *J Thorac Oncol* 5: 1120–1129

Bonecchi R, Borroni EM, Anselmo A, Doni A, Savino B, Mirolo M, Fabbri M, Jala VR, Haribabu B, Mantovani A, *et al* (2008) Regulation of D6 chemokine scavenging activity by ligand- and Rab11-dependent surface up-regulation. *Blood* 112: 493–503

Bontemps Y, Scamuffa N, Calvo F & Khatib A-M (2007) Potential opportunity in the development of new therapeutic agents based on endogenous and exogenous inhibitors of the proprotein convertases. *Med Res Rev* 27: 631–648

Boucher JM, Clark RP, Chong DC, Citrin KM, Wylie LA & Bautch VL (2017) Dynamic alterations in decoy VEGF receptor-1 stability regulate angiogenesis. *Nat Commun* 8: 15699

Buccafusca G, Proserpio I, Tralongo AC, Rametta Giuliano S & Tralongo P (2019) Early colorectal cancer: diagnosis, treatment and survivorship care. *Critical Reviews in Oncology/Hematology* 136: 20–30

Cazzato RL, Buy X, Alberti N, Fonck M, Grasso RF & Palussière J (2015) Flat-panel cone-beam CT-guided radiofrequency ablation of very small (≤ 1.5 cm) liver tumors: technical note on a preliminary experience. *Cardiovasc Intervent Radiol* 38: 206–212

Chen Z, Han F, Du Y, Shi H & Zhou W (2023) Hypoxic microenvironment in cancer: molecular mechanisms and therapeutic interventions. *Sig Transduct Target Ther* 8: 1–23

Davenport AP, Scully CCG, de Graaf C, Brown AJH & Maguire JJ (2020) Advances in therapeutic peptides targeting G protein-coupled receptors. *Nat Rev Drug Discov* 19: 389–413

Descarpentrie J, Araúzo-Bravo MJ, He Z, François A, González Á, Garcia-Gallastegi P, Badiola I, Evrard S, Pernot S, Creemers JWM, *et al* (2022) Role of Furin in Colon Cancer Stem Cells Malignant Phenotype and Expression of LGR5 and NANOG in KRAS and BRAF-Mutated Colon Tumors. *Cancers (Basel)* 14: 1195

El Messari S, Iturrioz X, Fassot C, De Mota N, Roesch D & Llorens-Cortes C (2004a) Functional dissociation of apelin receptor signaling and endocytosis: implications for the effects of apelin on arterial blood pressure. *J Neurochem* 90: 1290–1301

El Messari S, Iturrioz X, Fassot C, De Mota N, Roesch D & Llorens-Cortes C (2004b) Functional dissociation of apelin receptor signaling and endocytosis: implications for the effects of apelin on arterial blood pressure. *J Neurochem* 90: 1290–1301

Falcão-Pires I, Ladeiras-Lopes R & Leite-Moreira AF (2010) The apelinergic system: a promising therapeutic target. *Expert Opinion on Therapeutic Targets* 14: 633–645

Feng M, Yao G, Yu H, Qing Y & Wang K (2016) Tumor apelin, not serum apelin, is associated with the clinical features and prognosis of gastric cancer. *BMC Cancer* 16: 794

Gordon VM, Benz R, Fujii K, Leppla SH & Tweten RK (1997) Clostridium septicum alpha-toxin is proteolytically activated by furin. *Infect Immun* 65: 4130–4134

Gourgue F, Mignion L, Van Hul M, Dehaen N, Bastien E, Payen V, Leroy B, Joudiou N, Vertommen D, Bouzin C, *et al* (2020) Obesity and triple-negative-breast-cancer: Is apelin a new key target? *J Cell Mol Med* 24: 10233–10244

He L, Chen L & Li L (2016) The mechanosensitive APJ internalization via clathrin-mediated endocytosis: A new molecular mechanism of cardiac hypertrophy. *Medical Hypotheses* 90: 6–10

Henriet E, Abou Hammoud A, Dupuy J-W, Dartigues B, Ezzoukry Z, Dugot-Senant N, Leste-Lasserre T, Pallares-Lupon N, Nikolski M, Le Bail B, *et al* (2017) Argininosuccinate synthase 1 (ASS1): A marker of unclassified hepatocellular adenoma and high bleeding risk. *Hepatology* 66: 2016–2028

Hong C-S, Park M-R, Sun E-G, Choi W, Hwang J-E, Bae W-K, Rhee JH, Cho S-H & Chung I-J (2019) Gal-3BP Negatively Regulates NF-κB Signaling by Inhibiting the Activation of TAK1. *Front Immunol* 10: 1760

Humphries A & Wright NA (2008) Colonic crypt organization and tumorigenesis. *Nat Rev Cancer* 8: 415–424

Jean F, Stella K, Thomas L, Liu G, Xiang Y, Reason AJ & Thomas G (1998) alpha1-Antitrypsin Portland, a bioengineered serpin highly selective for furin: application as an antipathogenic agent. *Proc Natl Acad Sci USA* 95: 7293–7298

Kehoe K, Van Elzen R, Verkerk R, Sim Y, Van der Veken P, Lambeir A-M & De Meester I (2016) Prolyl carboxypeptidase purified from human placenta: its characterization and identification as an apelin-cleaving enzyme. *Biochim Biophys Acta* 1864: 1481–1488

Kojima Y & Quertermous T (2008) Apelin-APJ signaling in retinal angiogenesis. *Arterioscler Thromb Vasc Biol* 28: 1687–1688

Kurcinski M, Pawel Ciemny M, Oleniecki T, Kuriata A, Badaczewska-Dawid AE, Kolinski A & Kmiecik S (2019) CABS-dock standalone: a toolbox for flexible protein-peptide docking. *Bioinformatics* 35: 4170–4172

Lee DK, Cheng R, Nguyen T, Fan T, Kariyawasam AP, Liu Y, Osmond DH, George SR & O'Dowd BF (2000) Characterization of apelin, the ligand for the APJ receptor. *J Neurochem* 74: 34–41

Lee DK, Ferguson SSG, George SR & O'Dowd BF (2010) The fate of the internalized apelin receptor is determined by different isoforms of apelin mediating differential interaction with beta-arrestin. *Biochem Biophys Res Commun* 395: 185–189

Ljoki A, Aslam T, Friis T, Ohm RG & Houen G (2022) In Vitro Angiogenesis Inhibition and Endothelial Cell Growth and Morphology. *Int J Mol Sci* 23: 4277

Lv S, An Y, Dong H, Xie L, Zheng H, Cheng X, Zhang L, Teng T, Wang Q, Yan Z, *et al* (2022) High APLN Expression Predicts Poor Prognosis for Glioma Patients. *Oxid Med Cell Longev* 2022: 8393336

Ma Y, Yue Y, Ma Y, Zhang Q, Zhou Q, Song Y, Shen Y, Li X, Ma X, Li C, *et al* (2017) Structural Basis for Apelin Control of the Human Apelin Receptor. *Structure* 25: 858-866.e4

Masri B, Morin N, Cornu M, Knibiehler B & Audigier Y (2004) Apelin (65-77) activates p70 S6 kinase and is mitogenic for umbilical endothelial cells. *FASEB J* 18: 1909–1911

McKinnie SMK, Fischer C, Tran KMH, Wang W, Mosquera F, Oudit GY & Vederas JC (2016) The Metalloprotease Neprilysin Degrades and Inactivates Apelin Peptides. *Chembiochem* 17: 1495–1498

Morgan E, Arnold M, Gini A, Lorenzoni V, Cabasag CJ, Laversanne M, Vignat J, Ferlay J, Murphy N & Bray F (2023) Global burden of colorectal cancer in 2020 and 2040: incidence and mortality estimates from GLOBOCAN. *Gut* 72: 338–344

Palmer ES, Irwin N & O'Harte FP (2022) Potential Therapeutic Role for Apelin and Related Peptides in Diabetes: An Update. *Clin Med Insights Endocrinol Diabetes* 15: 11795514221074679

Perez-Riverol Y, Csordas A, Bai J, Bernal-Llinares M, Hewapathirana S, Kundu DJ, Inuganti A, Griss J, Mayer G, Eisenacher M, *et al* (2019) The PRIDE database and related tools and resources in 2019: improving support for quantification data. *Nucleic Acids Res* 47: D442–D450

Pettersen EF, Goddard TD, Huang CC, Meng EC, Couch GS, Croll TI, Morris JH & Ferrin TE (2021) UCSF ChimeraX: Structure visualization for researchers, educators, and developers. *Protein Sci* 30: 70–82

Picault F-X, Chaves-Almagro C, Projetti F, Prats H, Masri B & Audigier Y (2014a) Tumour co-expression of apelin and its receptor is the basis of an autocrine loop involved in the growth of colon adenocarcinomas. *Eur J Cancer* 50: 663–674

Picault F-X, Chaves-Almagro C, Projetti F, Prats H, Masri B & Audigier Y (2014b) Tumour co-expression of apelin and its receptor is the basis of an autocrine loop involved in the growth of colon adenocarcinomas. *Eur J Cancer* 50: 663–674

Piccolo E, Tinari N, D'Addario D, Rossi C, Iacobelli V, La Sorda R, Lattanzio R, D'Egidio M, Di Risio A, Piantelli M, *et al* (2015) Prognostic relevance of LGALS3BP in human colorectal carcinoma. *J Transl Med* 13: 248

Pitkin SL, Maguire JJ, Kuc RE & Davenport AP (2010) Modulation of the apelin/APJ system in heart failure and atherosclerosis in man. *Br J Pharmacol* 160: 1785–1795

Read C, Nyimanu D, Williams TL, Huggins DJ, Sulentic P, Macrae RGC, Yang P, Glen RC, Maguire JJ & Davenport AP (2019) International Union of Basic and Clinical Pharmacology. CVII. Structure and Pharmacology of the Apelin Receptor with a Recommendation that Elabela/Toddler Is a Second Endogenous Peptide Ligand. *Pharmacol Rev* 71: 467–502

Reaux A, De Mota N, Skultetyova I, Lenkei Z, El Messari S, Gallatz K, Corvol P, Palkovits M & Llorens-Cortès C (2001) Physiological role of a novel neuropeptide, apelin, and its receptor in the rat brain. *J Neurochem* 77: 1085–1096

Scamuffa N, Sfaxi F, Ma J, Lalou C, Seidah N, Calvo F & Khatib A-M (2014) Prodomain of the proprotein convertase subtilisin/kexin Furin (ppFurin) protects from tumor progression and metastasis. *Carcinogenesis* 35: 528–536

Scamuffa N, Siegfried G, Bontemps Y, Ma L, Basak A, Cherel G, Calvo F, Seidah NG & Khatib A-M (2008) Selective inhibition of proprotein convertases represses the metastatic potential of human colorectal tumor cells. *J Clin Invest* 118: 352–363

Seidah NG & Prat A (2012) The biology and therapeutic targeting of the proprotein convertases. *Nat Rev Drug Discov* 11: 367–383

Selvam S, Kumar T & Fruttiger M (2018) Retinal vasculature development in health and disease. *Progress in Retinal and Eye Research* 63: 1–19

Sfaxi F, Scamuffa N, Lalou C, Ma J, Metrakos P, Siegfried G, Ragg H, Bikfalvi A, Calvo F & Khatib A-M (2014) Repression of liver colorectal metastasis by the serpin Spn4A a naturally occurring inhibitor of the constitutive secretory proprotein convertases. *Oncotarget* 5: 4195–4210

Siegfried G, Descarpentrie J, Evrard S & Khatib A-M (2020) Proprotein convertases: Key players in inflammation-related malignancies and metastasis. *Cancer Lett* 473: 50–61

Siriwardena AK, Mason JM, Mullamitha S, Hancock HC & Jegatheeswaran S (2014) Management of colorectal cancer presenting with synchronous liver metastases. *Nat Rev Clin Oncol* 11: 446–459

Soulet F, Bodineau C, Hooks KB, Descarpentrie J, Alves I, Dubreuil M, Mouchard A, Eugenie M, Hoepffner J-L, López JJ, *et al* (2020) ELA/APELA precursor cleaved by furin displays tumor suppressor function in renal cell carcinoma through mTORC1 activation. *JCI Insight* 5: e129070, 129070

Sun X, Hu Y, Wu J, Shi L, Zhu L, Xi P-W, Wei J-F & Ding Q (2018) RBMS2 inhibits the proliferation by stabilizing P21 mRNA in breast cancer. *J Exp Clin Cancer Res* 37: 298

Takahashi S, Kasai K, Hatsuzawa K, Kitamura N, Misumi Y, Ikehara Y, Murakami K & Nakayama K (1993) A mutation of furin causes the lack of precursor-processing activity in human colon carcinoma LoVo cells. *Biochem Biophys Res Commun* 195: 1019–1026

Takano S, Uchida K, Inoue G, Matsumoto T, Aikawa J, Iwase D, Mukai M, Miyagi M & Takaso M (2018) Vascular endothelial growth factor expression and their action in the synovial membranes of patients with painful knee osteoarthritis. *BMC Musculoskelet Disord* 19: 204

Tang Z, Li C, Kang B, Gao G, Li C & Zhang Z (2017) GEPIA: a web server for cancer and normal gene expression profiling and interactive analyses. *Nucleic Acids Res* 45: W98–W102

del Toro R, Prahst C, Mathivet T, Siegfried G, Kaminker JS, Larrivee B, Breant C, Duarte A, Takakura N, Fukamizu A, *et al* (2010) Identification and functional analysis of endothelial tip cell-enriched genes. *Blood* 116: 4025–4033

Toyama BH & Hetzer MW (2013) Protein homeostasis: live long, won't prosper. *Nat Rev Mol Cell Biol* 14: 55–61

Versele M, Talloen W, Rockx C, Geerts T, Janssen B, Lavrijssen T, King P, Göhlmann HWH, Page M & Perera T (2009) Response prediction to a multitargeted kinase inhibitor in cancer cell lines and xenograft tumors using high-content tyrosine peptide arrays with a kinetic readout. *Mol Cancer Ther* 8: 1846–1855

Vickers C, Hales P, Kaushik V, Dick L, Gavin J, Tang J, Godbout K, Parsons T, Baronas E, Hsieh F, *et al* (2002) Hydrolysis of biological peptides by human angiotensin-converting enzyme-related carboxypeptidase. *J Biol Chem* 277: 14838–14843

Wang G, Anini Y, Wei W, Qi X, OCarroll A-M, Mochizuki T, Wang H-Q, Hellmich MR, Englander EW & Greeley GH (2004) Apelin, a new enteric peptide: localization in the gastrointestinal tract, ontogeny, and stimulation of gastric cell proliferation and of cholecystokinin secretion. *Endocrinology* 145: 1342–1348

Wang Y, Zhong X, He X, Hu Z, Huang H, Chen J, Chen K, Zhao S, Wei P & Li D (2023) Liver metastasis from colorectal cancer: pathogenetic development, immune landscape of the tumour microenvironment and therapeutic approaches. *Journal of Experimental & Clinical Cancer Research* 42: 177

Williams TL, Nwokoye P, Kuc RE, Smith K, Paterson AL, Allinson K, Maguire JJ & Davenport AP (2024) Expression of the apelin receptor, a novel potential therapeutic target, and its endogenous ligands in diverse stem cell populations in human glioblastoma. *Front Neurosci* 18: 1379658

Xu F, Xia T, Xu Q-T, Zhang X, Huang Y-Z, Sun X, Shi L, Zhou X-J, Wei J-F & Ding Q (2022) RBMS2 Chemosensitizes Breast Cancer Cells to Doxorubicin by Regulating BMF Expression. *Int J Biol Sci* 18: 1724–1736

Yang P, Read C, Kuc RE, Buonincontri G, Southwood M, Torella R, Upton PD, Crosby A, Sawiak SJ, Carpenter TA, *et al* (2017) Elabela/Toddler Is an Endogenous Agonist of the

Apelin APJ Receptor in the Adult Cardiovascular System, and Exogenous Administration of the Peptide Compensates for the Downregulation of Its Expression in Pulmonary Arterial Hypertension. *Circulation* 135: 1160–1173

Yue Y, Liu L, Wu L-J, Wu Y, Wang L, Li F, Liu J, Han G-W, Chen B, Lin X, *et al* (2022) Structural insight into apelin receptor-G protein stoichiometry. *Nat Struct Mol Biol* 29: 688–697

Zuurbier L, Rahman A, Cordes M, Scheick J, Wong TJ, Rustenburg F, Joseph JC, Dynoodt P, Casey R, Drillenburg P, *et al* (2017) Apelin: A putative novel predictive biomarker for bevacizumab response in colorectal cancer. *Oncotarget* 8: 42949–42961

Figure legends

Figure 1. Specific cleavage of apelin precursor (proapelin) by Furin and altered expression of apelin, Furin and apelin receptor in colon cancer and colorectal liver metastasis. A, Schematic representation of the primary structure of the 77 amino acid (aa), 55 aa and 36 aa of human apelin precursors and the maturated apelin-17 and apelin-13 aa peptides. The signal peptide (SP), the cleavage site of apelin-55 to apelin-36, and the two proprotein convertase (PCs)-processing sites are indicated (arrows). **B,** Proapelin processing by PCs was analyzed by immunoblotting in media of LoVo cells, a PCs activity-deficient cell line, that were co-transfected with empty vector (None), or vectors containing proapelin (Control) and indicated PCs cDNAs. **C,** Proapelin processing by Furin in media and lysates from CHO-FD11 cells with reduced Furin activity co-transfected with empty vector (None), or vectors containing preproapelin and/or Furin constructs, was analyzed by Western blotting. **D,** Inhibition of proapelin processing was assessed by Western blot analysis in media of HEK293A cells co-transfected with empty vector (None), or vectors containing preproapelin (Control) and indicated Furin inhibitors, or treated with the PC inhibitor decanoyl-Arg-Val-Lys-Arg-chloromethyl-ketone (CMK, 10μM). The bars show the corresponding percentage of band intensities deduced from the ratio of those of apelin/(proapelin + apelin) and indicate the level of mature apelin accumulation (%). Data are representative of 3 independent experiments and all values represent the mean±s.e.m. P values by two-tailed unpaired t-test. ns: not significant. **E-F,** Representative immunofluorescence images of colon cancer samples (CRC) and adjacent healthy tissues (Normal) from patients (n=35) that were stained with anti-apelin (red) and anti-Furin (green) **(E)** or with anti-apelin receptor (red) and anti-Furin (green) **(F)**. **G-H,** Representative images of apelin (red) and KI-67 (green) staining **(G)** and apelin receptor (red) and Furin (green) **(H)** staining in 35 CRC, mCRC and corresponding normal tissues. **I-J**, Plots of the correlation between KI-67 and apelin, KI-67 and apelin receptor, and KI-67 and Furin expression in CRC and mCRC that was determined by immunofluorescence following staining intensity analysis of G and H data, as measured on ImageJ and Spearman's correlation analysis. **K-M,** Relative expression of APLN **(K)**, APLNR **(L)** and Furin **(M)** mRNA in human normal colon (N colon), corresponding CRC and mCRC livers. Unpaired *t* tests were used to analyze the data. **N**, Kinetics of Furin mRNA accumulation in HUVEC cells cultured in normoxia (21% O_2) or hypoxia (1% O_2) for various time periods as indicated and data are representative of three independent experiments with values that represent the mean±s.e.m. Significant differences P were determined by Two-way ANOVA. Scale bar, 100 μm

Figure 2 Alteration of proapelin cleavage sites represses colorectal tumor growth and colorectal liver metastasis. A, Colon cancer cells CT-26 and MC-38 infected with lentivirus for stable expression of apelin and apelin-dm generated by mutation of the indicated PCs clevage sites $RR^{60}KFRR^{64}$ (arrows) and their processing were analyzed by Western blot analysis in the absence and presence of Furin (+/-). **B,** Experimental design of *in vivo* experiments, indicating subcutaneous and intraspleenc injected mice with CT-26 and MC-38 cells expressing apelin and apelin-dm and analysis of developed tumors. **C-E,** Tumor growth curves over time from representative experiment of subcutaneous inoculation of control CT-26 and MC-38 cells (10^{-6}) or the same cells stably expressing APLN and APLN-DM into Rag2/γ_c **(C)**, Balb/c **(D)** or Black6 **(E)** mice (*n*=8 tumors per group/experiment, 3 experiments). **F,** Representative images of livers from Black6 and BALB/c mice injected intrasplenically with control CT-26 and MC-38 cells or the same cells stably expressing APLN and APLN-DM (*n*=7 tumors per group/experiment, 3 experiments), respectively. In **C, D** and **E**, Error bars indicate s.e.m. center values indicate mean (Mann–Whitney U test). **G,** Number and incidence of liver nodules 15 days post intrasplenic injection (Mann-Whitney test). **H,** Representative immunofluorescence images

of liver tumor sections derived from control CT-26 cells or the same cells stably expressing APLN and APLN-DM that were stained with anti-Ki67 (proliferative index, red) and anti-CD31 (angiogenic index, green). Scale bar, 100 µm. **I-J**, The percentage of relative staining intensity (% RSI) of KI67, and CD-31 for control CT-26 tumors and CT-26 tumors expressing apelin and apelin-dm. Data are representative of 3 independent experiments as mean±s.e.m. P values by two-tailed unpaired t-test. **K,** Volcano plot of proteins in APLN and APLN-DM-expressing cells vs. Controls. Green dots indicate downregulated proteins; and red dots, upregulated proteins.**L,** Heat maps plotting expression of the 28 proteins inversely regulated between APLN and APLN-DM-expressing cells. **M,** *GSN, Spg20, NSUN5, APLN, APLNR* mRNA expression (Log_2 transcripts per million) in a panel of Colon adenocarcinoma (COAD) tissue specimens (n = 275) and normal samples (n = 349). Four-way ANOVA, using sex, age, ethnicity, and disease state, was used to calculate statistical significance. **N,** Correlation between expression of CYR61 and APLN, CYR61 and APLNR, RIC8A and APLN, and RIC8A and APLNR in colon adenocarcinoma. Data were derived from GEPIA(Tang *et al*, 2017). **O**, Schematic representation that summarizes APLN and APLN-DM regulated proteins associated with clinical outcome of colorectal cancer patients.

Figure 3. Apelin-dm peptide represses apelin-mediated vascular network and tumor cells malignant phenotype: Apelin-dm and apelin competition for apelin receptor binding. A, Amino acid sequences of apelin-13, apelin-17, apelin-36 and apelin-dm peptides. **B,** SDS gel analysis of wild type proapelin and apelin-dm peptide cleavage by Furin. Apelin-13 was added for comparaison. The difference in molecular weight and charge properties of the aa R and S in apelin-dm contributes to the lower migration of apelin-dm peptide than apelin-36. **C.** Furin expression analysis expressed as copy number per cell in smooth muscle cells (SMC), endothelial cells (HUVEC), and cancer cells CT-26 and MC-38 using droplet digital polymerase chain reaction (ddPCR) assay. **D,** Representative images of chick chorioallantoic membrane (CAM) treated for 48 h with apelin (100 nM) or/and apelin-dm (100nM) (n = 15). Small formed vessels are indicated by arrow heads. Quantification of vessel density is indicated in **E**. **F,** Representative image of Isolectin B4 staining in retinal whole mounts from 100 nM apelin, apelin-dm or apelin and apelin-dm-treated mice on P5. **G,** Quantification of retina vascularization, n = 6 total animals per group, from 3 different experiments. **H,** Representative images of CAM treated for 48 h with VEGF (30ng/ml) or/and apelin-dm (100nM**)** (n = 15). Small formed vessels are indicated by arrow heads. Quantification of vessel density is indicated in **I**. **J,** Cells were plated at low confluence for time-lapse phase-contrast videomicroscopy using an IncuCyte microscope, and cell proliferation in the presence of VEGF (30 ng/ml) or apelin-dm (100nM) was monitored by automated confluence analysis at set intervals after plating (means, n = 6 wells per group, 3 independent experiments). **K**, Effect of apelin-dm (100 nM) on VEGF (30ng/ml)-induced migration of HUVECs. **M**, Effect of apelin-dm (100nM) on VEGF (30ng/ml)-induced ERK phosphorylation in HUVEC cells analyzed by immunoblotting. **N,** Quantification of ERK phosphorylation relative to control untreated HUVEC assigned 100%. **L**, Anchorage independent colony formation assay was performed on colon cancer cells HT-29 in the presence of apelin and/or apelin-dm. **O**, The number of colony>100µm were counted and the results were presented as the percentage of the developed colonies. **P**, Effect of apelin peptides and/or apelin-dm on the migration of colon cancer cells CT-26. All data are representative of three independent experiments. All values represent the mean±s.e.m. Significant differences *P* were determined by Two-way ANOVA. scales, 500 µm. **Q**, Docking peptides into apelin receptor. A representative binding poses for apelin-dm (red) is shown, with the C-terminal region inserted in the main binding pocket (allosteric site 1), while the N- terminal region seemed to wrap around the receptor. The predicted structure of the apelin-36 and apelin receptor is highly similar and is not shown to simplify the figure. The two Furin cleavage sites are shown.

All apelin peptides are predicted to interact with another allosteric pocket (allosteric site 2) while only apelin-36 or apelin-dm is likely to contact yet another allosteric binding pocket (allosteric site 3). Colored spheres (yellow) show the predicted position of the membrane. Inset, apelin-17 and apelin-13 were also docked into the receptor and numerous contacts between these peptides and the protein are lost as compared to apelin-dm and apelin-36. **R**, Apelin-apelin receptor docking scores per-residue and global binding energy scores. The per-residue decomposition of apelin-dm (or apelin-36) docking score is shown (the per-residue scores between the two peptides are very similar). Each dot represents an amino acid, the color code is assigned according to the predicted binding score with apelin receptor for each residue. Only some residues are predicted to contribute significantly to the binding with the receptor (e.g., the C-term F). The approximate total interaction energy values for each peptide and the receptor are also shown. **S-U**, Plasmon waveguide resonance (PWR). Binding curve for apelin (**S**), and apelin-dm (**T**) interaction with apelin receptor in HEK-apelin receptor . **U**, plots showing the results of KD values (n = 3) corresponding to **S** and **T**. **V,** Conformational changes of apelin receptor in response to apelin and apelin-dm. Spectral changes induced by apelin and apelin-dm binding to apelin receptor with two polarizations (p-pol and s-pol) (n=3). P: p- (perpendicular to the sensor surface) polarized light S: s- (parallel to the sensor surface). In U and V, data are representative of 3 independent experiments and shown as the mean±s.e.m. Significant differences P determined by 1-way ANOVA with Tukey's multiple comparison tests.

Figure 4. Effect of apelin-dm on apelin receptor internalization and signaling, and Kinome profiling.

A, Representative images of Fluorescence microscopy used to visualize β-arrestin 2-GFP recruitment to the human apelin receptor in U2OS cells stably co-transfected with apelin receptor and pEGFP-β-arrestin2 in the absence and presence of apelin-Tamara and/or apelin-dm. **B,** Representative images of clathrin staining (red) and β-arrestin 2-GFP (green) recruitment to the human apelin receptor in U2OS cells in the absence and presence of apelin and apelin-dm. **C,** Radioligand binding assay. Apelin receptor membrane extracts were incubated with [125I]-(Pyr1)-apelin-13 in the presence of various concentration of apelin-13 or apelin-dm. **D**, KD values (n = 3) of apelin, apelin-dm and apelin-dm/Elabela generated by plasmon waveguide resonance (PWR). **E**, Effect of apelin-dm (100nM) on ERK phosphorylation in HEK cells-expressing apelin receptor induced by Elabela (100 nM). **F-G,** Phosphorylation of AKT (**F**) and ERK (**G**) analyzed by immunoblotting of HUVEC cells treated with apelin and apelin-dm. Data are representative of 3 independent experiments and data shown as the mean±s.e.m. Significant differences P determined by 1-way ANOVA with Tukey's multiple comparison tests. **H-I**, heatmaps showing log2-transformed signal intensities for 196 PTK (**H**) peptide substrates and 144 STK (**I**) peptide substrates phosphorylated of Control, apelin and apelin-dm-treated HEK cells-expressing apelin receptor. The signals were sorted from high (red) to low (blue) intensity/phosphorylation. **J-K**, Changes in peptide phosphorylation in apelin and apelin-dm-treated HEK cells-expressing apelin receptor, analysed by a two-group comparison depicted as a volcano plot (effect size <0: less phosphorylation in treated cells; significance score (log2) >1.3 indicates significant changes, dotted line). **L-M**, Upstream kinase analysis of PTK (**L**) and STK (**M**) of control, apelin and apelin-dm-treated HEK cells-expressing apelin receptor showing the top 20 ranked kinases (normalized kinase statistic (log2) < 0: less kinase activity in treated cells; specificity score (log2) >1.3; white to red bars: statistically significant changes).

Figure 5. Therapeutic efficacy of apelin-dm. A, Scheme and workflow of apelin-dm preclinic studies. **B-D,** Tumor growth analysis of subcutaneously injected mice (*n*=8 tumors per group/experiment, 3 experiments) with CT-26 **(B)** and MC-38 **(C)** colon cancer cells treated with apelin-dm (30 mg/Kg), as shown in **A**. The apelin receptor antgonoist ML221 (30 µg/kg)**,** was used for comparaison **(D)**. In **B, C** and **D**, Error bars indicate s.e.m. center values indicate mean

(Mann–Whitney U test). **E-H,** Representative immunofluorescence staining of tumor sections derived from **B** and **C** shows CD31 (**E**, H green); KI-67 **(F**(green), **H** (red)); and BIM (apoptotic index, **G**, red). The percentage of relative staining intensity corresponding to CD31, Ki67, and BIM expression in CT-26 and MC-38 tumors of treated mice are shown in **I-N**. Data represent mean ± sem of 3-4 independent experiments. P values were calculated with the Student t test in GraphPad. **O**, Representative images of apelin and apelin-dm peptide effect on tumor growth and capillaries-treated CAMs implanted with CT-26 colon cancer cells (n = 6 per group). Scale bar, 100 µm. Quantification of tumor area **(P)** and vascularized area **(Q)** relative to control untreated CAMs assigned 100%. Data represent mean ± sem. P values were calculated with the Student t test in GraphPad. **R**, color-coded images of blood flow analyzed by laser Doppler imager in control, apelin-dm (30mg/Kg) and Bevacizumab (5mg/Kg)-treated mice tumors. **S-T**, The average blood flow expressed in % relatively to blood flow measured in HCT113 **(S)** and MDA MB231**(T)** developed tumors. Data represent mean ± sem of 3-4 independent experiments. P values were calculated with the Student t test in GraphPad.

Figure 6. Apelin-dm peptide represses early events of colorectal liver metastasis. RT-PCR **(A, C-F)** and immunostaining **(B)** analyses of E-selectin expression in human liver sinusoidal endothelial cells (LSEC), HMEC-1, and HUVEC treated with 100 nM each of apelin, apelin-dm, and/or MM54 (n = 3 per group, 3 independent experiments). Values represent the mean ± s.e.m., and significant differences (P) were determined by two-way ANOVA. **G**, Scheme and workflow of apelin-dm effect analysis on E-selectin expression and metastasis induced by colon cancer cells CT-26 and MC-38 (10^6). **H-I**, Mice were injected through the intrasplenic/portal route with 10^6 CT-26 cells and treated with apelin-dm **(H)** or MM54 **(I)** (30 mg/Kg), as shown in **G**. Their livers were then removed for E-selectin mRNA expression analysis (n = 6 per group). Results shown are representative of 3 experiments. Values are mean ± sem. P values were calculated using the Student's t-test in GraphPad. **J**, Representative images of livers from mice (n = 7 tumors per group/experiment) injected intrasplenically with control CT-26 treated with apelin-dm and MM54 (30 mg/Kg), as shown in G. The number and incidence of liver nodules 2 weeks after tumor cell injection were evaluated **(K).** Data are representative of 3 independent experiments as mean ± s.e.m., and the Mann–Whitney U test was used to examine statistical significance. Scale bar for B, 100 µm.

Figure 7. A model depicting apelin-dm interaction with the apelin receptor, leading to the repression of colon tumor angiogenesis and metastasis. Proapelin cleavage by Furin, which may occur at the tumor cell surface or in the Trans-Golgi Network (1), generates secreted mature apelin that activates the apelin receptor (2), inducing its internalization (3) and recycling (4) or degradation (5), leading to tumor growth, angiogenesis, survival, invasion, and metastasis (6). In contrast, apelin-dm interferes with the interaction and signaling between apelin and the apelin receptor (7), delaying or preventing apelin receptor recycling at the cell surface (8) and inhibiting these processes (9). All model diagrams were created using BioRender.com.

Figure 8. Workflow **(A)** and analysis **(B)** of the Absorption, Distribution, Metabolism, Excretion (ADME), Pharmacokinetics (PK), and Toxicity of apelin-dm (Details are provided in Appendix pharmacological study 1-4). MTD: The maximum tolerated dose.

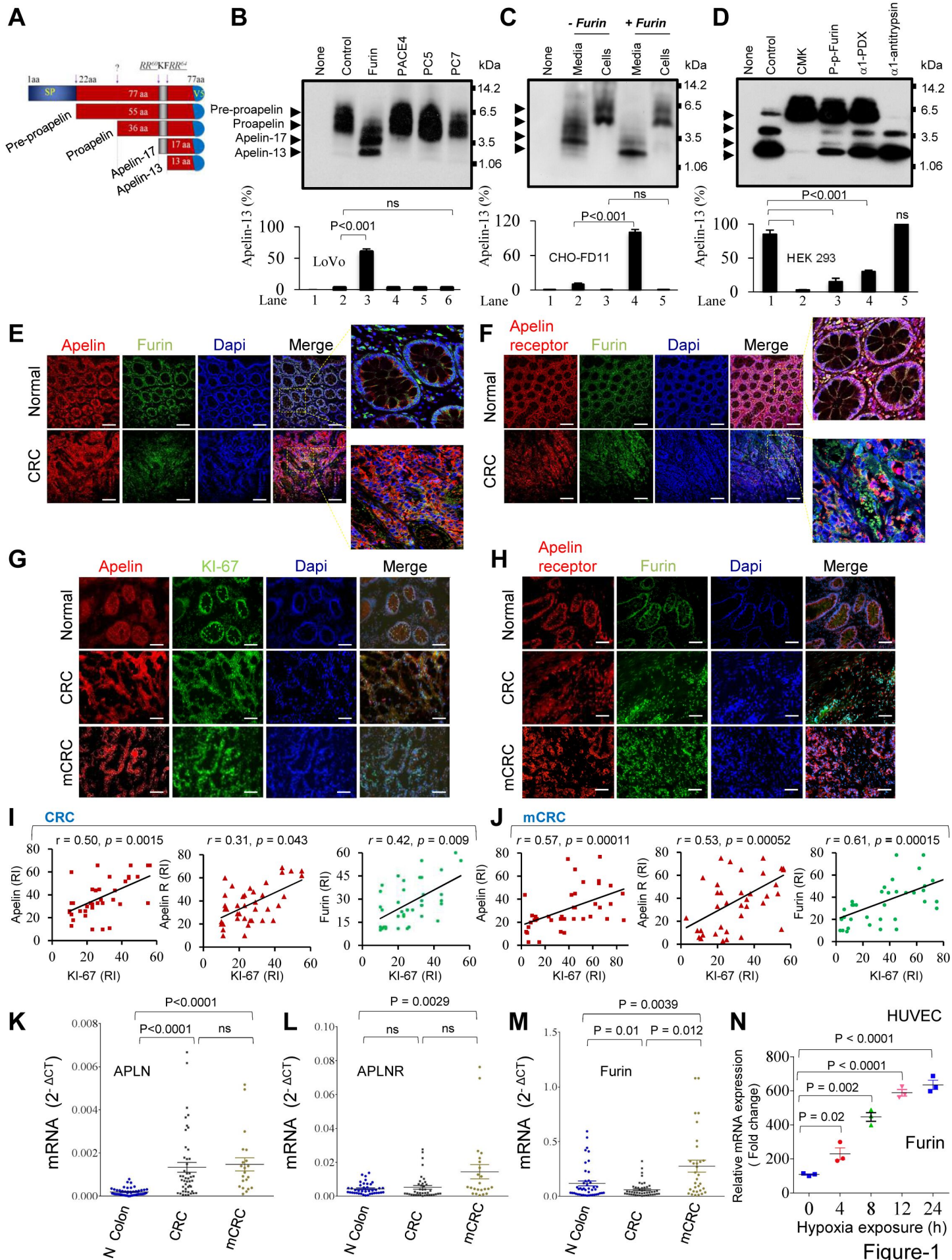
A
Pre-proapelin
Proapelin
Apelin-17
Apelin-13
SP
77 aa
55 aa
36 aa
17 aa
13 aa
1aa
22aa
77aa
B
None
Control
Furin
PACE4
PC5
PC7
kDa
14.2
6.5
3.5
1.06
Pre-proapelin
Proapelin
Apelin-17
Apelin-13
Apelin-13 (%)
LoVo
P<0.001
ns
Lane
C
- Furin
+ Furin
Media
Cells
CHO-FD11
D
CMK
P-p-Furin
α1-PDX
α1-antitrypsin
HEK 293
E
Apelin
Furin
Dapi
Merge
Normal
CRC
F
Apelin receptor
G
KI-67
mCRC
H
I
CRC
r = 0.50, p = 0.0015
r = 0.31, p = 0.043
r = 0.42, p = 0.009
Apelin (RI)
Apelin R (RI)
Furin (RI)
KI-67 (RI)
J
mCRC
r = 0.57, p = 0.00011
r = 0.53, p = 0.00052
r = 0.61, p = 0.00015
K
APLN
mRNA (2- ΔCT)
N Colon
L
APLNR
M
Furin
N
HUVEC
Relative mRNA expression (Fold change)
Hypoxia exposure (h)

Figure-1

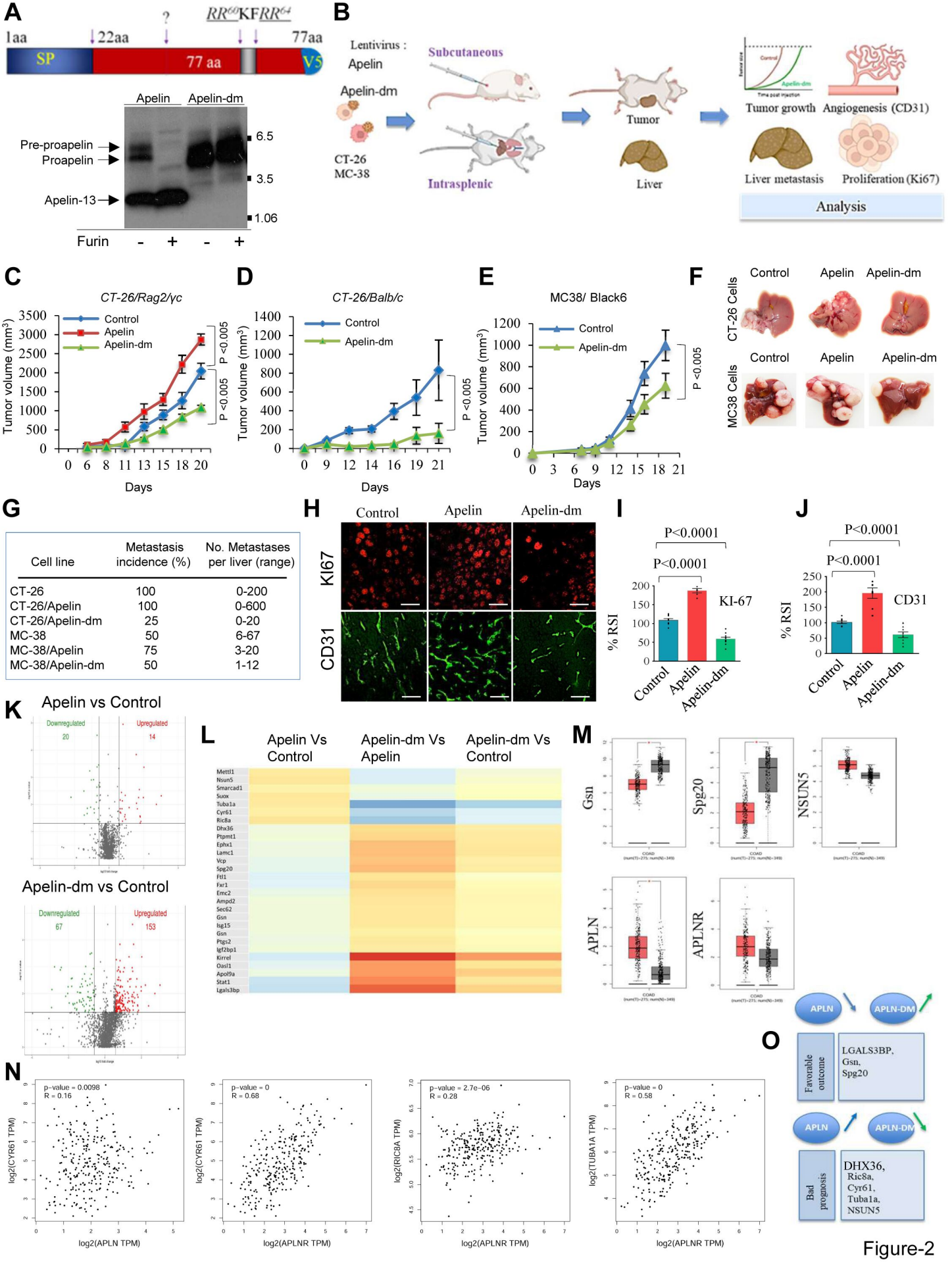
A
1aa
22aa
77aa
SP
77 aa
V5
Apelin
Apelin-dm
Pre-proapelin
Proapelin
Apelin-13
6.5
3.5
1.06
Furin - + - +
B
Lentivirus :
Apelin
Apelin-dm
CT-26
MC-38
Subcutaneous
Intrasplenic
Tumor
Liver
Tumor growth
Angiogenesis (CD31)
Liver metastasis
Proliferation (Ki67)
Analysis
C
CT-26/Rag2/γc
Control
Apelin
Apelin-dm
Tumor volume (mm3)
P <0.005
P <0.005
Days
D
CT-26/Balb/c
Control
Apelin-dm
Tumor volume (mm3)
P <0.005
Days
E
MC38/ Black6
Control
Apelin-dm
Tumor volume (mm3)
P <0.005
Days
F
Control
Apelin
Apelin-dm
CT-26 Cells
MC38 Cells
G
Cell line | Metastasis incidence (%) | No. Metastases per liver (range)
CT-26 | 100 | 0-200
CT-26/Apelin | 100 | 0-600
CT-26/Apelin-dm | 25 | 0-20
MC-38 | 50 | 6-67
MC-38/Apelin | 75 | 3-20
MC-38/Apelin-dm | 50 | 1-12
H
Control
Apelin
Apelin-dm
KI67
CD31
I
P<0.0001
P<0.0001
% RSI
KI-67
Control
Apelin
Apelin-dm
J
P<0.0001
P<0.0001
% RSI
CD31
Control
Apelin
Apelin-dm
K
Apelin vs Control
Downregulated
20
Upregulated
14
Apelin-dm vs Control
Downregulated
67
Upregulated
153
L
Apelin Vs Control
Apelin-dm Vs Apelin
Apelin-dm Vs Control
Mettl1
Nsun5
Smarcad1
Suox
Tuba1a
Cyr61
Ric8a
Dhx36
Ptpmt1
Ephx1
Lamc1
Vcp
Spg20
Ftl1
Fxr1
Emc2
Ampd2
Sec62
Gsn
Isg15
Gsn
Ptgs2
Igf2bp1
Kirrel
Oasl1
Apol9a
Stat1
Lgals3bp
M
Gsn
Spg20
NSUN5
APLN
APLNR
COAD
N
p-value = 0.0098
R = 0.16
log2(CYR61 TPM)
log2(APLN TPM)
p-value = 0
R = 0.68
log2(CYR61 TPM)
log2(APLNR TPM)
p-value = 2.7e-06
R = 0.28
log2(RIC8A TPM)
log2(APLNR TPM)
p-value = 0
R = 0.58
log2(TUBA1A TPM)
log2(APLNR TPM)
O
APLN
APLN-DM
Favorable outcome
LGALS3BP, Gsn, Spg20
APLN
APLN-DM
Bad prognosis
DHX36, Ric8a, Cyr61, Tuba1a, NSUN5

Figure-2

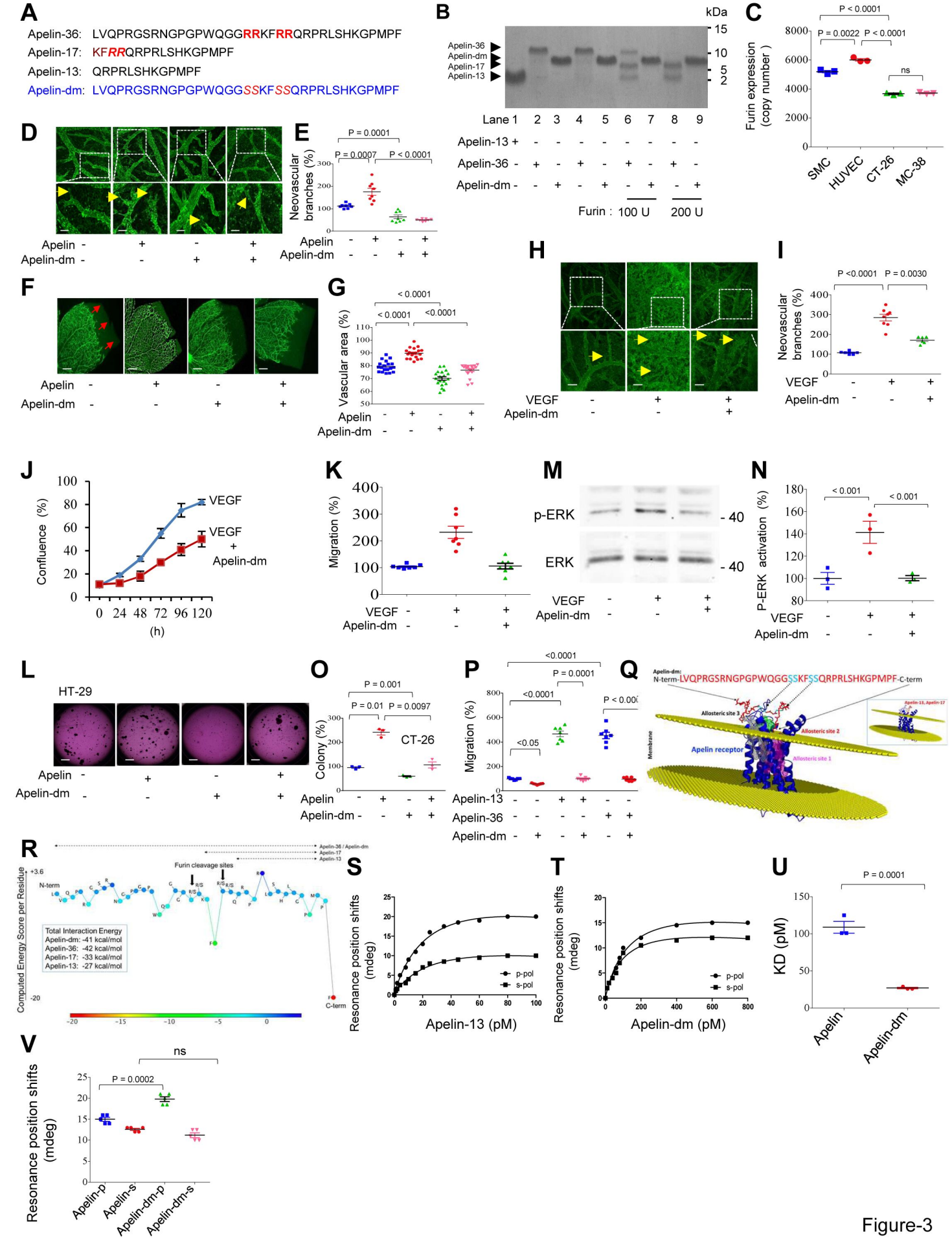
A
Apelin-36: LVQPRGSRNGPGPWQGGRRKFRRQRPRLSHKGPMPF
Apelin-17: KFRRQRPRLSHKGPMPF
Apelin-13: QRPRLSHKGPMPF
Apelin-dm: LVQPRGSRNGPGPWQGGSSKFSSQRPRLSHKGPMPF
B
kDa
Apelin-36
Apelin-dm
Apelin-17
Apelin-13
Lane 1 2 3 4 5 6 7 8 9
Apelin-13 + - - - - - - - -
Apelin-36 - + - + - + - + -
Apelin-dm - - + - + - + - +
Furin : 100 U 200 U
C
Furin expression (copy number)
P < 0.0001
P = 0.0022
P < 0.0001
ns
SMC
HUVEC
CT-26
MC-38
D
Apelin - + - +
Apelin-dm - - + +
E
Neovascular branches (%)
P = 0.0001
P = 0.0007
P < 0.0001
Apelin - + - +
Apelin-dm - - + +
F
Apelin - + - +
Apelin-dm - - + +
G
Vascular area (%)
< 0.0001
< 0.0001
<0.0001
Apelin - + - +
Apelin-dm - - + +
H
VEGF - + +
Apelin-dm - - +
I
Neovascular branches (%)
P <0.0001
P = 0.0030
VEGF - + +
Apelin-dm - - +
J
Confluence (%)
VEGF
VEGF + Apelin-dm
0 24 48 72 96 120
(h)
K
Migration (%)
VEGF - + +
Apelin-dm - - +
M
p-ERK
ERK
- 40
- 40
VEGF - + +
Apelin-dm - - +
N
P-ERK activation (%)
< 0.001
< 0.001
VEGF - + +
Apelin-dm - - +
L
HT-29
Apelin - + - +
Apelin-dm - - + +
O
Colony (%)
P = 0.001
P = 0.01
P = 0.0097
CT-26
Apelin - + - +
Apelin-dm - - + +
P
Migration (%)
<0.0001
P = 0.0001
<0.0001
<0.05
P < 0.00
Apelin-13 - - + + - -
Apelin-36 - - - - + +
Apelin-dm - + - + - +
Q
Apelin-dm:
N-term-LVQPRGSRNGPGPWQGGSSKFSSQRPRLSHKGPMPF-C-term
Allosteric site 3
Allosteric site 2
Allosteric site 1
Apelin receptor
Membrane
Apelin-13, Apelin-17
R
Apelin-36 / Apelin-dm
Apelin-17
Apelin-13
Furin cleavage sites
+3.6
N-term
C-term
-20
Computed Energy Score per Residue
Total Interaction Energy
Apelin-dm: -41 kcal/mol
Apelin-36: -42 kcal/mol
Apelin-17: -33 kcal/mol
Apelin-13: -27 kcal/mol
S
Resonance position shifts (mdeg)
p-pol
s-pol
Apelin-13 (pM)
T
Resonance position shifts (mdeg)
p-pol
s-pol
Apelin-dm (pM)
U
KD (pM)
P = 0.0001
Apelin
Apelin-dm
V
Resonance position shifts (mdeg)
ns
P = 0.0002
Apelin-p
Apelin-s
Apelin-dm-p
Apelin-dm-s

Figure-3

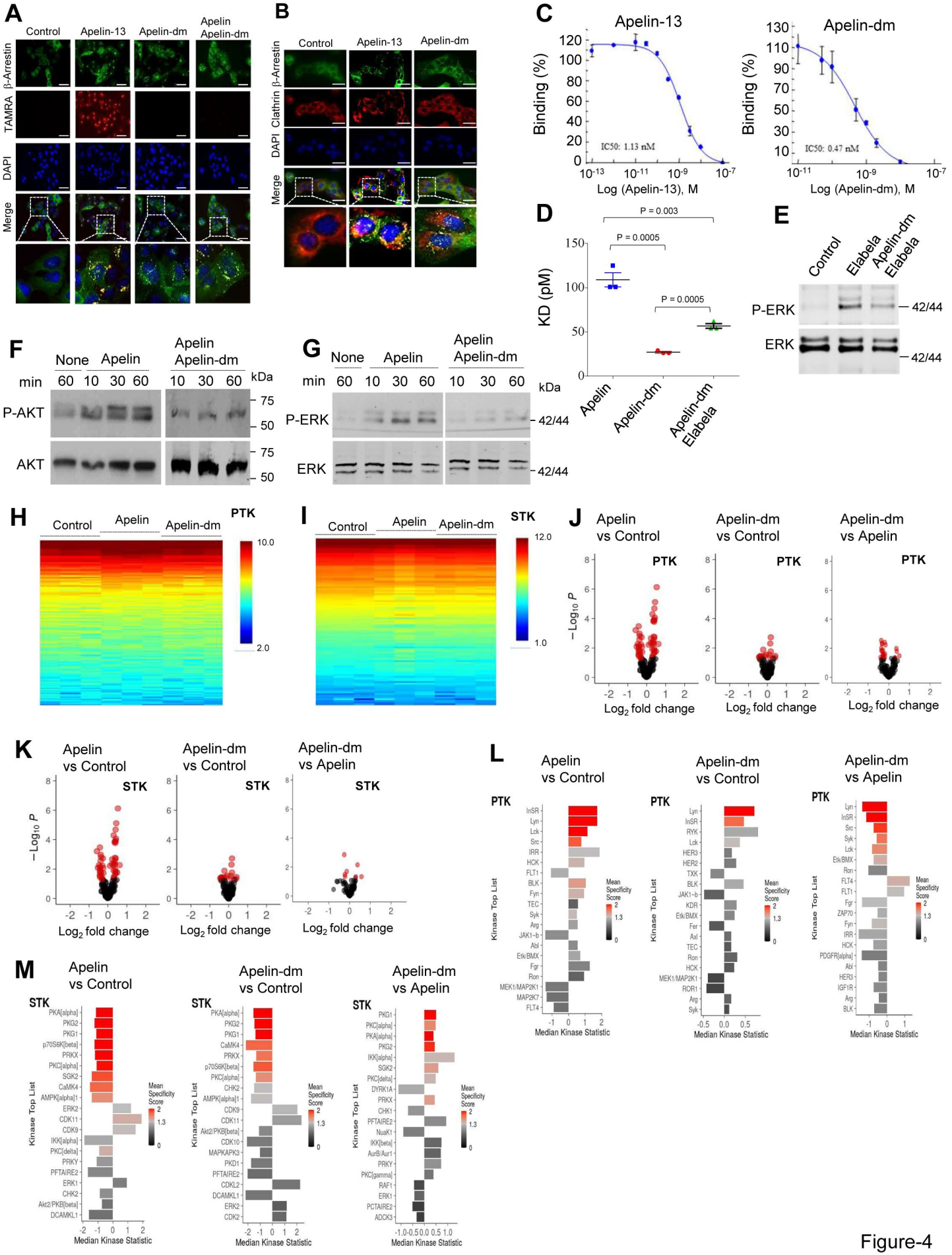
A
Control
Apelin-13
Apelin-dm
Apelin
Apelin-dm
β-Arrestin
TAMRA
DAPI
Merge
B
Control
Apelin-13
Apelin-dm
β-Arrestin
Clathrin
DAPI
Merge
C
Apelin-13
Binding (%)
IC50: 1.13 nM
Log (Apelin-13), M
Apelin-dm
IC50: 0.47 nM
Log (Apelin-dm), M
D
P = 0.003
P = 0.0005
P = 0.0005
KD (pM)
Apelin
Apelin-dm
Apelin-dm Elabela
E
Control
Elabela
Apelin-dm
Elabela
P-ERK
ERK
42/44
42/44
F
None
Apelin
Apelin
Apelin-dm
min
60
10
30
60
10
30
60
kDa
P-AKT
AKT
75
50
75
50
G
None
Apelin
Apelin
Apelin-dm
min
60
10
30
60
10
30
60
kDa
P-ERK
ERK
42/44
42/44
H
Control
Apelin
Apelin-dm
PTK
10.0
2.0
I
Control
Apelin
Apelin-dm
STK
12.0
1.0
J
Apelin
vs Control
Apelin-dm
vs Control
Apelin-dm
vs Apelin
PTK
PTK
PTK
−Log10 P
Log2 fold change
Log2 fold change
Log2 fold change
K
Apelin
vs Control
Apelin-dm
vs Control
Apelin-dm
vs Apelin
STK
STK
STK
−Log10 P
Log2 fold change
Log2 fold change
Log2 fold change
L
Apelin
vs Control
Apelin-dm
vs Control
Apelin-dm
vs Apelin
PTK
PTK
PTK
Kinase Top List
Mean Specificity Score
Median Kinase Statistic
Median Kinase Statistic
Median Kinase Statistic
M
Apelin
vs Control
Apelin-dm
vs Control
Apelin-dm
vs Apelin
STK
STK
STK
Kinase Top List
Mean Specificity Score
Median Kinase Statistic
Median Kinase Statistic
Median Kinase Statistic

Figure-4

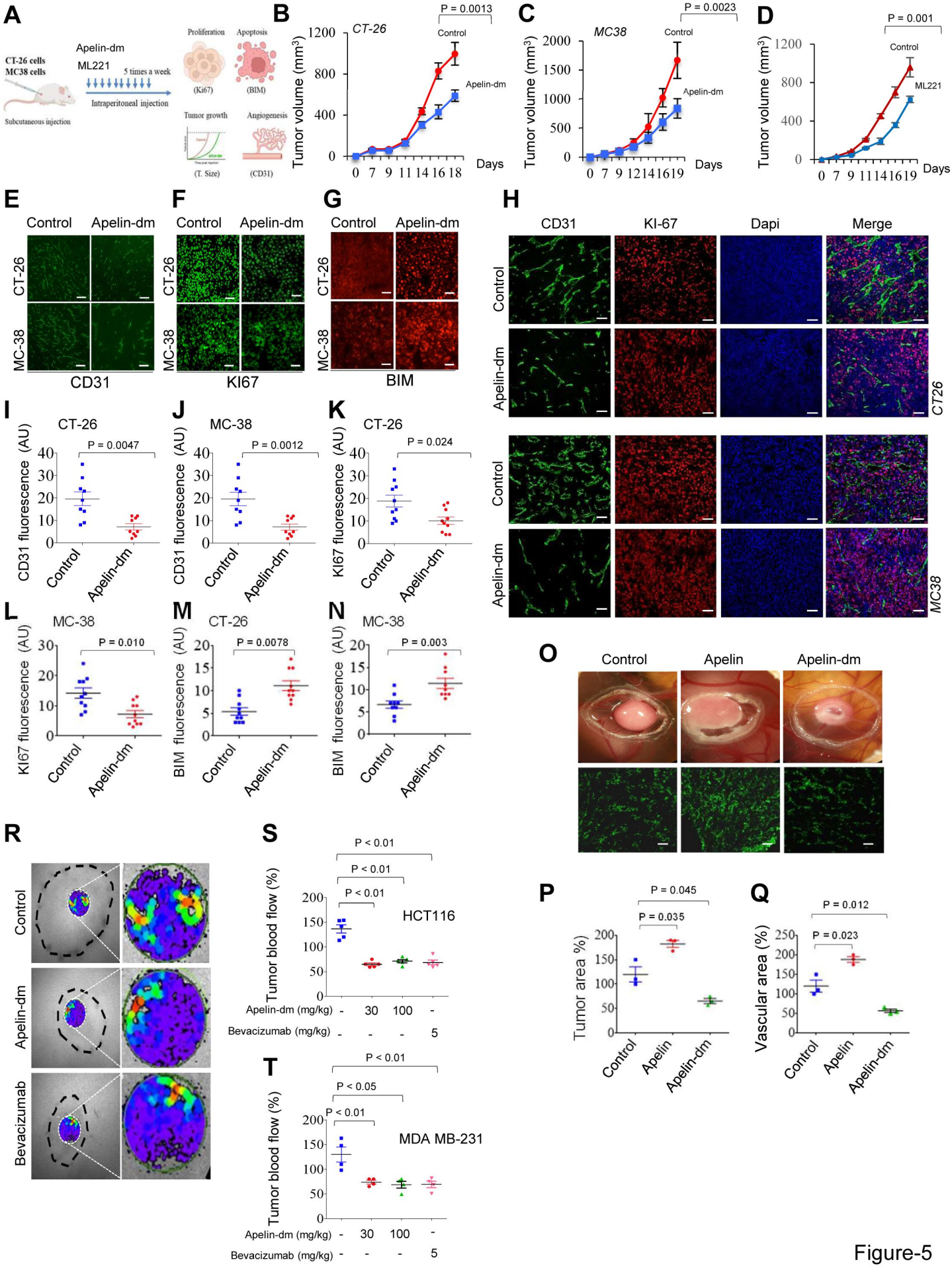
A
CT-26 cells
MC38 cells
Subcutaneous injection
Apelin-dm
ML221
5 times a week
Intraperitoneal injection
Proliferation
Apoptosis
(Ki67)
(BIM)
Tumor growth
Angiogenesis
(T. Size)
(CD31)
B
CT-26
P = 0.0013
Control
Apelin-dm
Tumor volume (mm3)
Days
C
MC38
P = 0.0023
Control
Apelin-dm
Tumor volume (mm3)
Days
D
P = 0.001
Control
ML221
Tumor volume (mm3)
Days
E
Control
Apelin-dm
CT-26
MC-38
CD31
F
Control
Apelin-dm
CT-26
MC-38
KI67
G
Control
Apelin-dm
CT-26
MC-38
BIM
H
CD31
KI-67
Dapi
Merge
Control
Apelin-dm
CT26
Control
Apelin-dm
MC38
I
CT-26
P = 0.0047
CD31 fluorescence (AU)
Control
Apelin-dm
J
MC-38
P = 0.0012
CD31 fluorescence (AU)
Control
Apelin-dm
K
CT-26
P = 0.024
KI67 fluorescence (AU)
Control
Apelin-dm
L
MC-38
P = 0.010
KI67 fluorescence (AU)
Control
Apelin-dm
M
CT-26
P = 0.0078
BIM fluorescence (AU)
Control
Apelin-dm
N
MC-38
P = 0.003
BIM fluorescence (AU)
Control
Apelin-dm
O
Control
Apelin
Apelin-dm
P
P = 0.045
P = 0.035
Tumor area %)
Control
Apelin
Apelin-dm
Q
P = 0.012
P = 0.023
Vascular area (%)
Control
Apelin
Apelin-dm
R
Control
Apelin-dm
Bevacizumab
S
P < 0.01
P < 0.01
P < 0.01
HCT116
Tumor blood flow (%)
Apelin-dm (mg/kg) - 30 100 -
Bevacizumab (mg/kg) - - - 5
T
P < 0.01
P < 0.05
P < 0.01
MDA MB-231
Tumor blood flow (%)
Apelin-dm (mg/kg) - 30 100 -
Bevacizumab (mg/kg) - - - 5

Figure-5

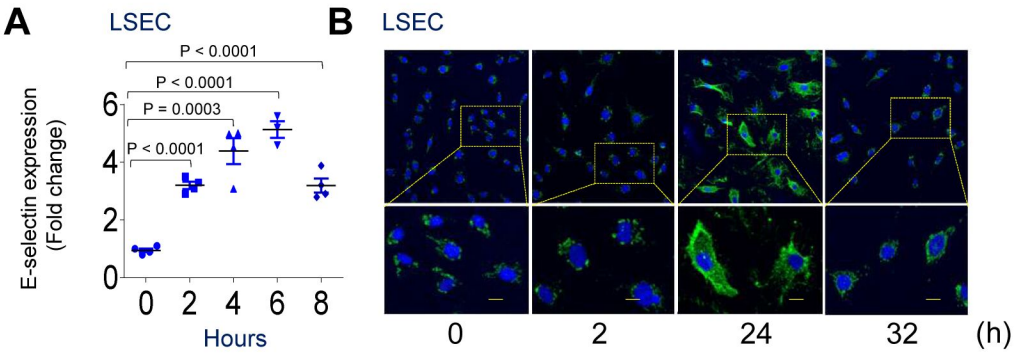

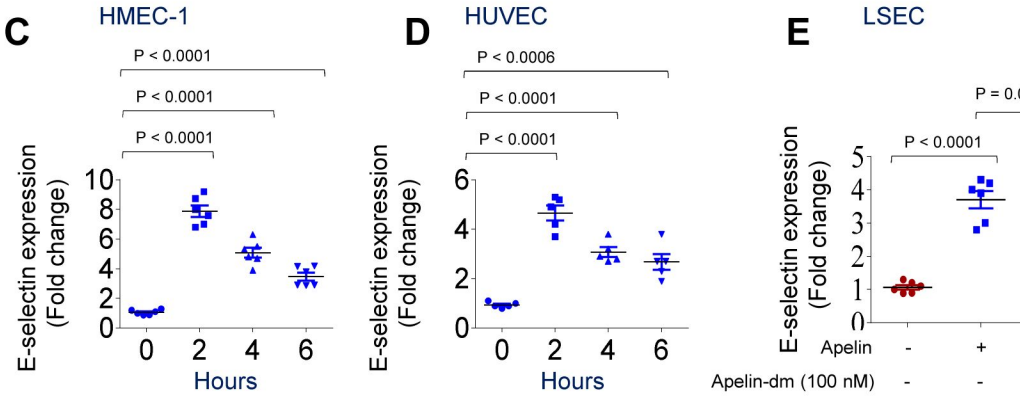

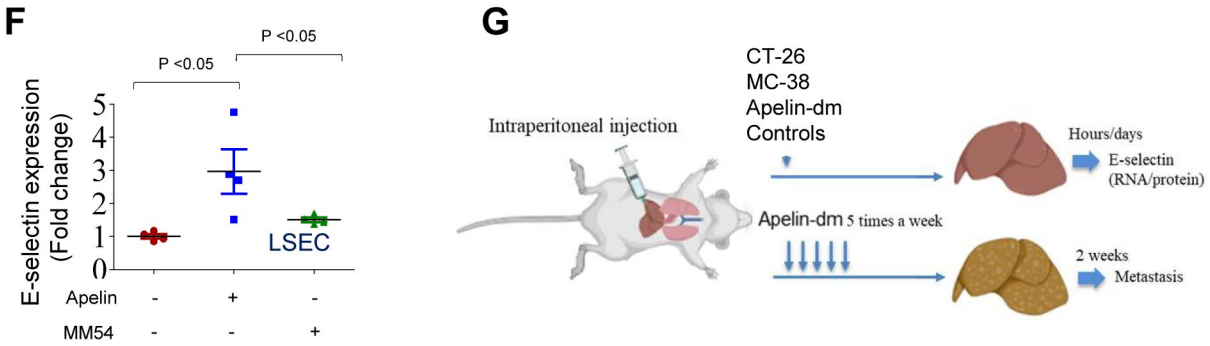

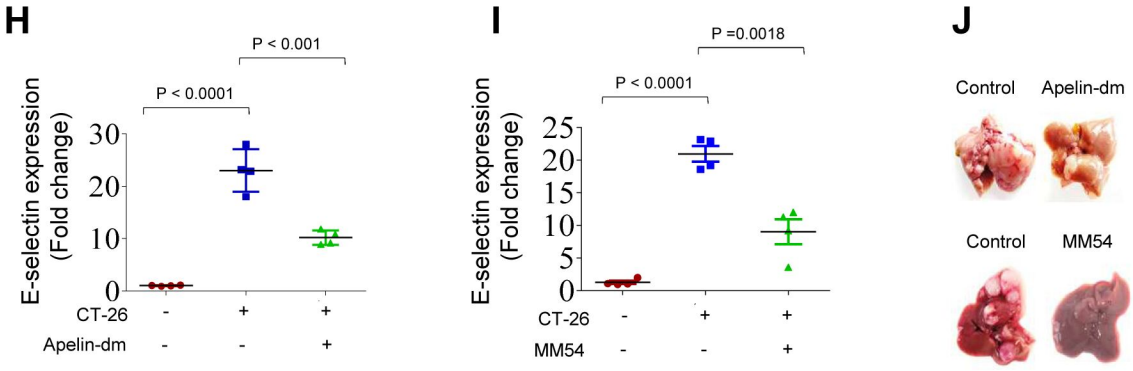

K

	Metastasis incidence (%)	No. Metastases per liver (range)
Control	100	60-300
Apelin-dm	50	0-200
Control	100	3-100
MM54	60	0-22

Figure-6

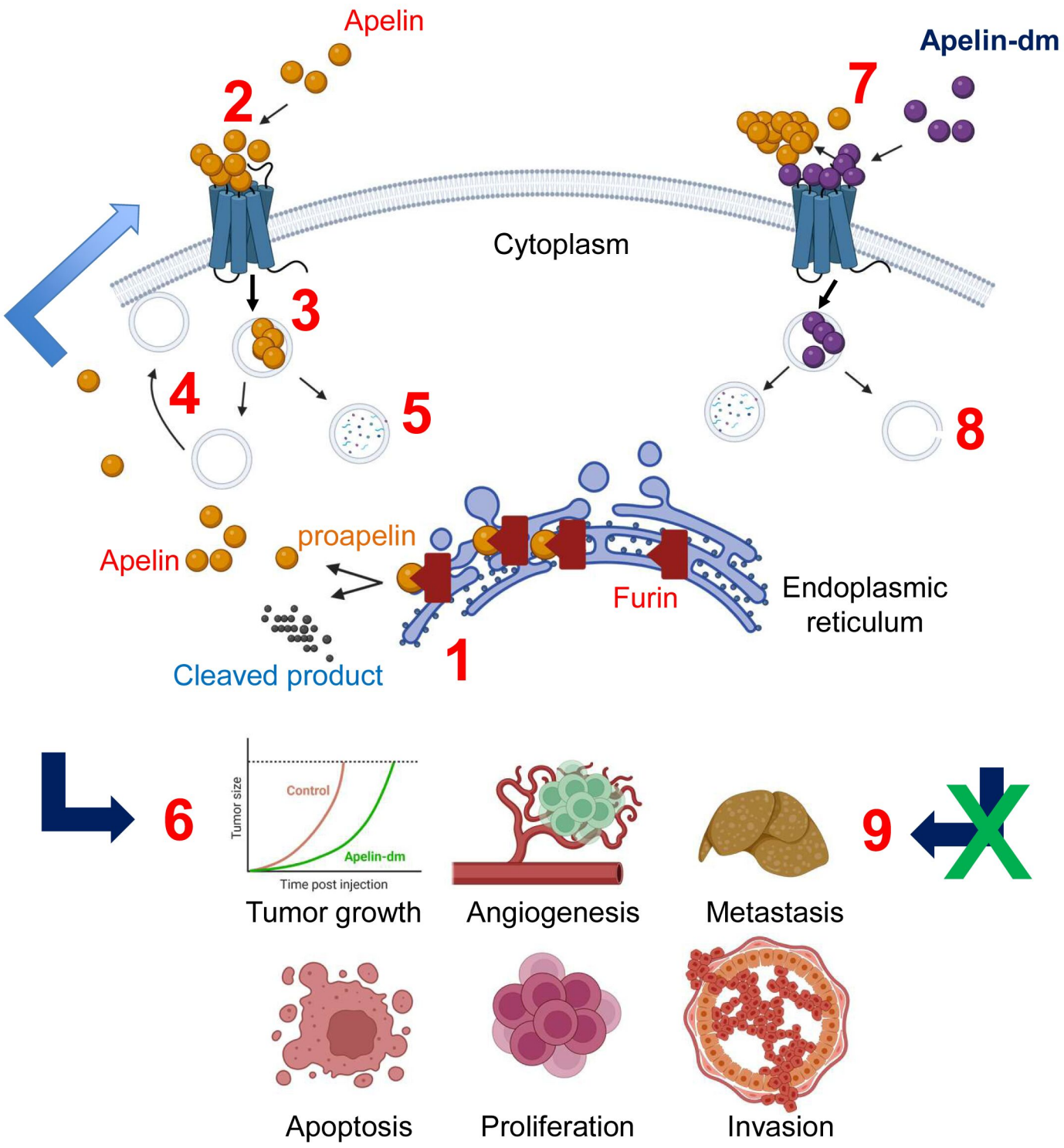
Apelin
Apelin-dm
2
7
Cytoplasm
3
4
5
8
Apelin
proapelin
Furin
Endoplasmic reticulum
Cleaved product
1
6
Tumor size
Control
Apelin-dm
Time post injection
9
Tumor growth
Angiogenesis
Metastasis
Apoptosis
Proliferation
Invasion

Figure-7

A

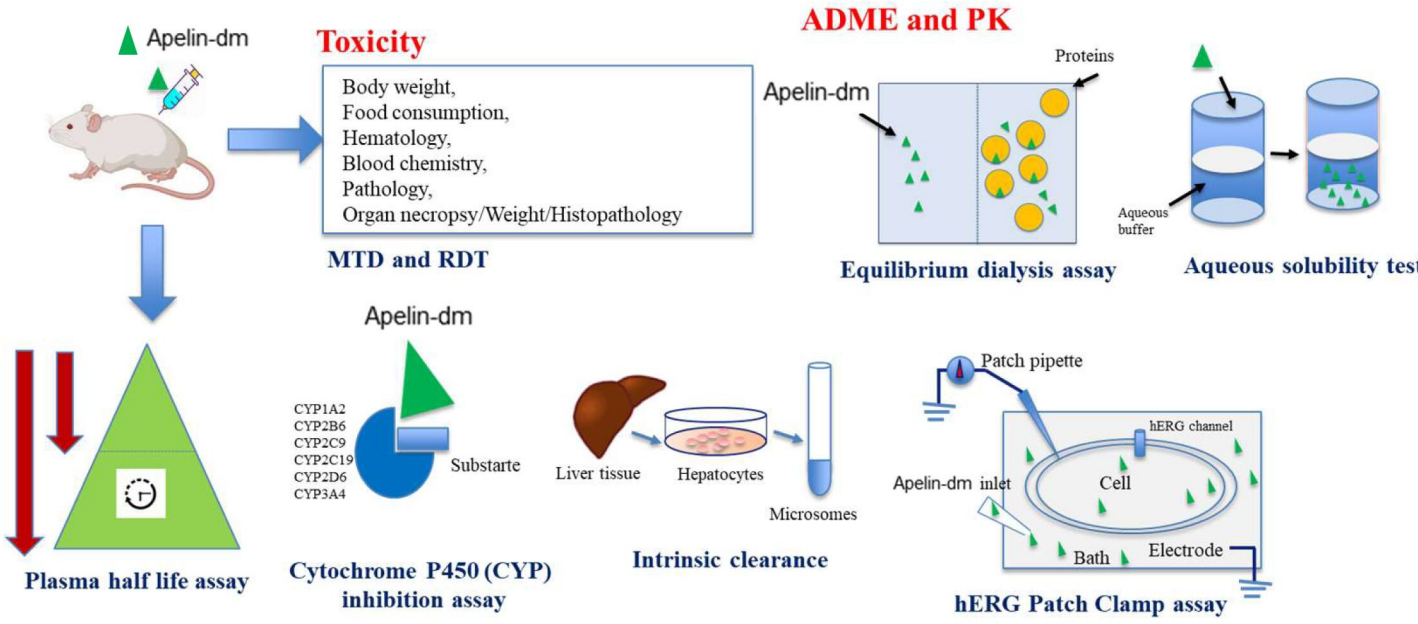

B

Pharmacological evaluation	Calculated values	Detailed study in:
MTD		
Acute toxicity	>1000 mg/kg	Appendix pharmacological study 1
Repeated administrations	300 mg/kg/day for 14 days	Appendix pharmacological study 2
Half-life		Appendix pharmacological study 3
In vivo in Mice	20 min	
In human plasma	1121 min	
Protein bound assay (10^{-5} M)		Appendix pharmacological study 4
In human plasma	54%	
In mice plasma	26%	
Solubility (10^{-4} M)	187.3 µM	Appendix pharmacological study 4
Intrinsic clearance (10^{-7}M)	<115.5µL/min/mg	Appendix pharmacological study 4
CYP inhibition	CYP3A4 isoform	Appendix pharmacological study 4
Inhibition of the hERG current		Appendix pharmacological study 4
10^{-5} M	10.9%	
10^{-6} M	5.2%	
10^{-7} M	5.0%	

Figure-8